Ultrasound Controlled Drug Delivery by Acoustically Switchable Hydrogels

Thesis by

Maria Paulene Bernal Abundo

In Partial Fulfillment of the Requirements for

the degree of

Doctor of Philosophy

CALIFORNIA INSTITUTE OF TECHNOLOGY

Pasadena, California

2023

(Defended May 22, 2023)

Maria Paulene Abundo
ORCID: 0000-0002-5122-6937

ACKNOWLEDGEMENTS

I would like to thank my advisor, Prof. Mikhail Shapiro. Mikhail has made a profound impact on my life. Aside from the research assistance and support, Mikhail was the resilience, self-confidence, and courage that I needed when I had none. There were a lot of things that did not quite go as planned in my graduate journey, however, I know that being mentored by Mikhail was the best decision I have made for myself. So, thank you Mikhail for being a great advisor and fostering an incredible lab.

Next, I would like to thank the people I worked closely with for whom none of this would have been possible. Thank you, Anna, for being the best undergrad I could have mentored, for always sharing with me a slice of your (undergraduate) life and for being so brave to try new things. I don't think I could have found the courage to do animal experiments without seeing your calmness and confidence with animal handling. Thank you, Marjorie, for providing me with so much help and wisdom on animal gut experiments, and for single-handedly carrying me through days and nights of rodent imaging and data analysis. You inspire me with your dedication to research. Lastly, I am grateful to Pierina, Zhi yang, JK, Dina and Margaret for supporting all my miscellaneous experimental work.

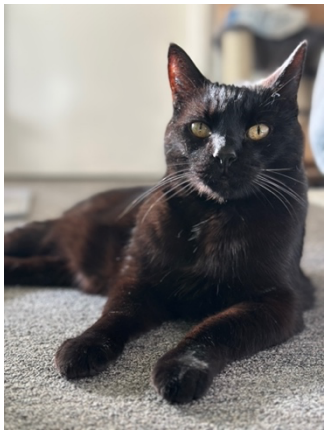

I would also like to thank my friends and family for their support. All of you have supported me through very strange circumstances both in my life and in the world, with the pandemic and lockdowns happening at such a critical juncture in my research.

And lastly, I would like to thank my cat, Zun. My time with you was short but sweet. You walked into my life when I was lonely, and left right after I was able to stand on my own feet.

ABSTRACT

Not only is ultrasound widely used as a diagnostic imaging modality, it can also be focused into deep tissues to perform non-invasive actuation of cells, implants and delivery vehicles and other biological targets. With the addition of gas vesicles (GV), generic hydrogel materials gain the ability to communicate with ultrasound, equipping them with *in vivo* tracking, targeting and actuation capabilities to safely transport biomolecular cargo. This is possible as GVs function simultaneously as ultrasound contrast agents and steric blockers that can be "erased" by an increase in ultrasound pressure to trigger a rapid outflow diffusion of the payload from within the material. We evaluate this concept through *in vitro* measurements of ultrasound-modulated diffusion and drug release and targeted *in vivo* release in the lower gastrointestinal tract. Then we demonstrate the use of orally administered hydrogel particles to deliver etanercept in the duodenum to treat gastrointestinal inflammation in a rat model of colitis. Finally, we explore new directions and applications of GV-hydrogel systems, showcasing their potential for deployment in a wide range of biomedical applications.

PUBLISHED CONTENT AND CONTRIBUTIONS

"Biomolecular actuators for genetically selective acoustic manipulation of cells" published by Wu D., Baresch D., Cook C., Ma Z., Duan M., Malounda D., Maresca D., Abundo M.P., Lee J., Shivaei S., Mittelstein D., Qiu T., Fischer P. and Shapiro M.G. in *Science Advances*,

DOI: https://doi.org/10.1126/sciadv.add9186

- Abundo M.P contributed to the microfluidic and acoustic radiation force experiments, and also to manuscript writing.

"Modular stimuli-responsive hydrogel sealants for early gastrointestinal leak detection and containment" published by Anthis A.H.C., Abundo M.P., Neuer A.L., Tsolaki E., Rosendorf J., Rduch T., Starsich F.H.L, Weisse B., Liska V., Schlegel A.A., Shapiro M.G. and Hermann I.K. in *Nature Communications*

DOI: https://doi.org/10.1038/s41467-022-34272-y

- Abundo M.P contributed to the design of the TurnOFF sensor used in the experiments and contributed to the manuscript writing.

TABLE OF CONTENTS

Acknowledgements……...iii
Abstract ……iv
Published Content and Contributions…….....v
Table of Contents……..vi
List of Illustrations and/or Tables……vii
Chapter I: Ultrasound Imaging, Targeting and Triggering in Drug Delivery Systems 1
1.1 Introduction 1
1.2 General Principles of Ultrasound.....2
1.2.1 Ultrasound B-mode Imaging 2
1.2.2 Contrast Imaging.....4
1.3 Ultrasound Actuation *in vivo* 6
1.3.1 Heat Dissipation 8
1.3.1.1 Limitations 9
1.3.2 Cavitation 10
1.3.2.1 Limitations 11
1.3.3 Acoustic Radiation Force.....12
1.3.3.1 Limitations 13
1.4 Contrast Agents and Sonosensitizers.....14
1.4.1 Microbubbles.....14
1.4.2 Metal and Inorganic Particles 14
1.4.3 Gas Vesicles 15
1.5 References 16

Chapter II: Ultrasound Controlled Drug Delivery by Acoustically Switchable Hydrogels.....21
2.1 Abstract 21
2.2 Introduction 22
2.3 GV-containing hydrogels exhibit acoustically switchable biomolecular diffusivity.....23
2.4 DASH devices enable imaging and spatially targeted on-demand drug release *in vitro* 28
2.5 DASH gels enable spatially selective ultrasound-triggered drug release *in vivo*.....31
2.6 DASH release of etanercept enables the treatment of colitis in an animal model.....39
2.7 Discussion 41
2.8 Methods.....47
2.9 Supplementary Data.....51
2.9 References 56

Chapter III: Ultrasound Controlled Smart GV-Hydrogel Systems 56
3.1 Abstract 56
3.2 Introduction 57
3.3 GV-gels enable acoustically multiplexed payload release 58
3.4 GV-gels can be tuned to deliver payloads across length scales 62
3.5 GVs enable biomaterial patterning using acoustic radiation force 66
3.6 GVs embedded in sealants enable post-surgical leak detection with ultrasound 71
3.7 References 76

LIST OF ILLUSTRATIONS AND/OR TABLES

Number *Page*

1–1 Properties and applications of ultrasound waves 4

1–2 Regimes of biomolecular ultrasound 6

T–1 Biologically relevant ultrasound attenuation coefficients 7

1–3 Liposomes for ultrasound-triggered drug delivery 8

1–4 Using cavitation to control drug release from liposomes 10

1–5 Cavitation regimes 11

1–6 Streaming effects from ARF are used to exert shear on lipid bilayer 12

2–1 GV-gels produce ultrasound-modulated diffusivity changes 26

2–2 DASH enables in vitro spatially targeted payload release with ultrasound-modulated release kinetics 29

2–3 In vivo spatially targeted imaging and payload release from GV-gels 32

2–4 GV-gels for oral delivery of biomolecules 35

2–5 GV-gels for the treatment of colitis in Sprague-Dawley rats using etanercept 38

2–S1 Negative control for BURST imaging 48

2–S2 Weight gain trends for healthy rats and rats with colitis 49

2–S3 Dosing experiment 50

3–1 Acoustic multiplexing using different GV variants 60

3–2 GV-gels enable acoustically multiplexed BSA diffusivity 61

3–3 Classes of therapeutic and delivery paradigms 63

3–4 Gas vesicle development and appearance 64

3–5 Ultrasound imaging of gene expression in mammalian cells 64

3–6 GV-gels produce ultrasound modulated diffusivity effects in a wide size range of solute and polymer candidates 65

3–7 GVs as biomolecular transducers of ARF 68

3–8 Dynamic patterning and one-step bioprinting with acoustic bacteria 69

3–9 Schematic of leak-detecting sealant hydrogel patches 72

3–10 Ultrasound imaging of TurnOFF hydrogel patch with GV elements 74

C h a p t e r I

ULTRASOUND IMAGING, TARGETING AND TRIGGERING IN DRUG DELIVERY SYSTEMS

1.1 Introduction

The field of drug delivery has witnessed remarkable progress, with smart vehicles now capable of executing a multitude of complex functions within the body. The primary objective of drug delivery systems is to enhance therapeutic efficacy by efficiently transporting and releasing drugs at the site of disease while minimizing off-target effects. To achieve this, it is essential for most delivery vehicles to possess a set of key abilities, including monitoring (via imaging), targeting, and triggering of drug release wirelessly. Most modern drug delivery systems (DDS) rely on the integration of imaging modalities, which work in conjunction with sensing, motor, or actuation components within the device. However, common methods for achieving precise interactions with DDS, such as through electric and magnetic fields, are challenging to focus in vivo, or by electromagnetic radiation which has limited utility in deep tissues. Ultrasound waves on the other hand can penetrate the body up to several centimeters deep and maintain high spatiotemporal resolutions of 100 μm and 0.1 ms respectively, making it widely used in medical imaging and in the noninvasive treatment of conditions like kidney stones[1]. Recent advancements have even allowed ultrasound to be coupled with intra-cellular processes, enabling real-time visualization and modulation of biological processes *in vivo*. It would be interesting if a similar analogy can be applied to the development of acoustically responsive materials for drug delivery, allowing sound to communicate directly with the vehicles to enable image-tracking, or the creation of acoustically active polymer microarchitectures.

In this chapter, we aim to provide a general understanding of ultrasound physics as a foundation for exploring its applications in drug delivery systems. We will begin by presenting the necessary background knowledge to grasp the principles of ultrasound. Then we will discuss several mechanisms of actuation which can be exploited in the release step.

Finally, we will be discussing the potential of some common ultrasound contrast agents and actuators, and assess the likelihood of them being incorporated in materials for drug delivery applications.

1.2 General Principles of Ultrasound

Ultrasound refers to frequencies of sound waves greater than 20 MHz, typically outside the audible range of humans. They are generated by probes or transducers which propagates the wave through a medium, with a certain initial energy and momentum. These sound waves interact with objects in its path via scattering or reflection (**Fig. 1a**), and the extent to which this occurs at an interface is determined by a material property called the acoustic impedance[2], Z:

$$Z = \sqrt{\rho\beta} \tag{1}$$

where ρ is the density and β is the compressibility or elastic stiffness of the material. Typical values of the acoustic impedance in biological systems can be found in **Table 1**.

In the body, it is relatively challenging to tell tissues apart from one another using ultrasound without anatomical context due to their similarities in acoustic impedance. However, air and bones have much lower and higher acoustic impedances respectively than water or tissues[3], allowing us to discern anatomical information based on strong reflections at these surfaces. These reflections are directional and reveal geometrical information regarding the surface, enabling the use of ultrasound as a diagnostic imaging modality. Due to its widespread use, many imaging modes for ultrasound have been created and translated into medical practice; two of them which are relevant to the use of macroscopic drug delivery systems will be discussed.

1.2.1 Ultrasound B-mode Imaging

B-mode, or brightness mode imaging, is the most basic mode of ultrasound imaging. It involves sending a short ultrasound pulse using a transducer, and listening for the arrival time and the amplitude of the backscattered echoes produced from the interfaces encountered by

the sound wave. These two pieces of information are then used to determine the position and intensity of a point on a 2D grayscale image (**Fig. 1d**).

For such images, there lies a tradeoff between resolution and signal attenuation. Resolution refers to the minimum distance that can be differentiated between two scatterers located parallel (axial) or perpendicular (transverse) to the direction of the ultrasound beam[4] whereas attenuation refers to the loss in signal intensity (or amplitude) as it propagates through a medium. Both are important parameters that must be optimized to enable gathering of precise spatiotemporal information, which will be relevant for delivery vehicle tracking and triggering.

The resolution λ is determined by:

$$\lambda = \frac{c_{tissue}}{f} \tag{2}$$

where c_{tissue} is the speed of sound in tissue and f is frequency of the ultrasound wave,

and attenuation can be mathematically visualized by:

$$I = I_0 e^{-\mu x} \tag{3}$$

$$\mu \propto f \tag{4}$$

where I is the transmitted amplitude, I_0 is the incident amplitude, x is the depth and μ is the absorption coefficient which varies linearly with frequency.

Since both resolution and attenuation increases with frequency, there results a tradeoff between resolution and depth (**Fig. 1c**). B-mode imaging is used to image most tissues with the exception of bones or air-filled organs such as the lungs[5].

1.2.2 Contrast Imaging

Contrast imaging refers to the use of contrast agents, which are scatterers with a markedly different acoustic impedance from its surroundings, to selectively label regions of interest. Some examples of commonly used contrast agents include microbubbles[6–9], various metal particles[10], and gas vesicles[5,11–13]. These will be discussed and evaluated at a later section.

Some contrast agents like gas vesicles, are capable of being imaged using non-linear imaging modes. These non-linear imaging modes arise due to the higher frequency back scattered echoes as a result of non-linear responses (e.g. buckling) to a propagating sound wave[47–48]. This imaging mode is useful for imaging in the body as most scatterers are linear like soft tissues.

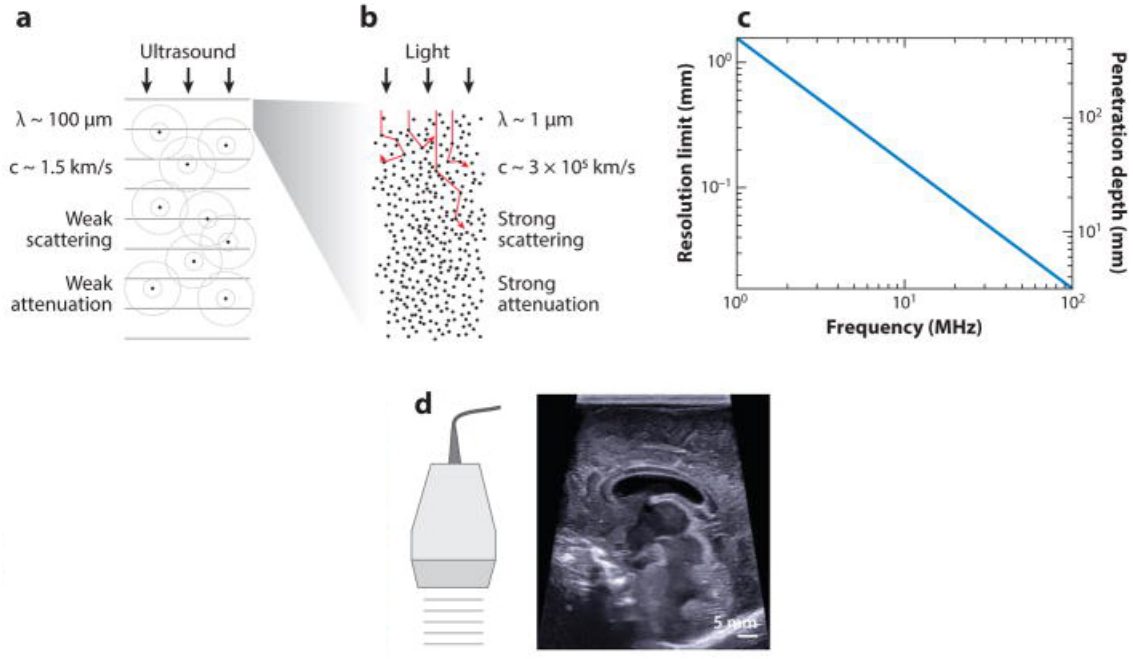

Figure 1 – Adapted and reproduced from Maresca D., et al (2018)[5], Properties and applications of ultrasound waves.

a, Physical properties of ultrasound waves in biological tissues. **b,** Physical properties of light traveling in biological tissue. **c,** Fundamental tradeoff between ultrasound resolution and penetration depth as a function of frequency in brain tissue (penetration depth was assessed based on a 60-decibel round-trip attenuation). At an ultrasound frequency of 15 MHz, one can expect to image the brain 2 cm deep at a 100-μm resolution. **d,** Illustration of ultrasound imaging capabilities; conventional B-mode image of an infant brain with a submillimeter resolution of cerebral structures

1.3 Ultrasound Actuation *in vivo*

Due to the low attenuation coefficient in soft tissues (Table 1), energy can be delivered to specific locations in the body using focused ultrasound (fUS) via three modes namely, heat dissipation, exertion of ARF, and acoustic cavitation[5,14] (**Fig. 2**). These actuation mechanisms have been frequently utilized in various drug delivery contexts and will be discussed next.

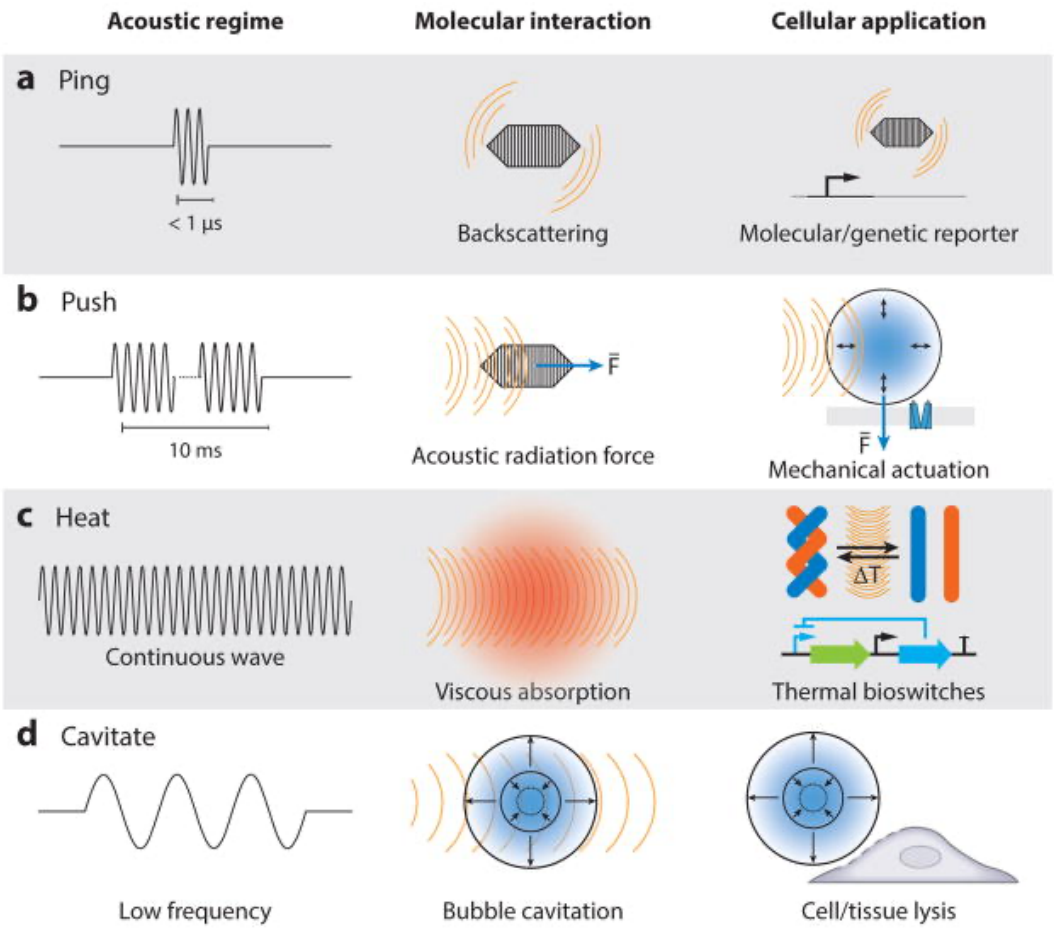

Figure 2 – Reproduced from Maresca D., et al (2018)[5], Regimes of biomolecular ultrasound.

Table 1 – Biologically relevant ultrasound attenuation coefficients[15]

Tissue / Medium	Attenuation Coefficient (dB/cm/MHz)	Acoustic Impedance (Mrayl)
Water	0.0022	1.5
Blood	0.15	1.6
Soft Tissue	0.75	1.6
Air	7.50	0.00001
Bone	15.0	8
Fat	0.63	1.4

1.3.1 Heat Dissipation

When ultrasound is focused into a viscous fluid, friction occurs due to the movement and collision of the fluid molecules resulting in local heating effects that increase with frequency and intensity[5]. This effect of concentrating mechanical energy into a focal spot with pulse durations on the order of seconds, results in substantial temperature increases called hyperthermia. It is routinely used to resolve uterine fibroids[16,17] and tumors[18–20].

In drug delivery, shorter pulse durations are typically used to trigger milder temperature changes. Most commonly used in 100 nm liposomal carriers[21–23], ultrasound is used to slightly elevate the body temperature to around 39–40 °C to trigger a phase transition in the liposomes (**Fig. 3**). This causes the permeability of the liposome shell to increase and release its stored payload over time. These local heating effects can also be exploited by heat-sensitive polymers[24] in hydrogel stimulus-based drug delivery systems to passively trigger small thermal expansions in the material that will increase outward solute diffusivity.

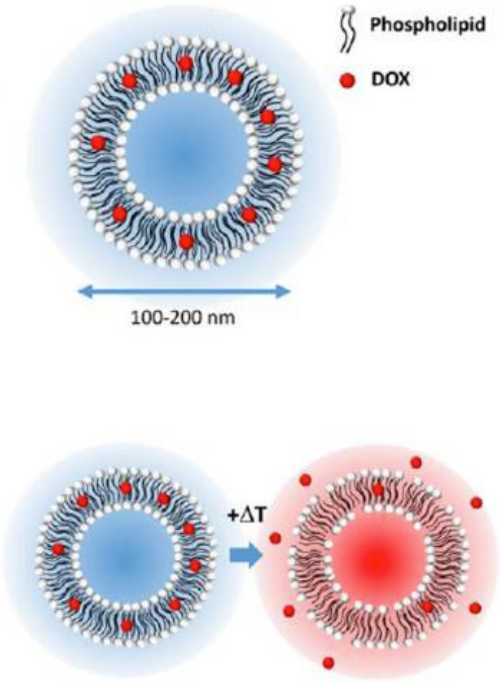

Figure 3 – Adapted and reproduced from Sirsi S. and Borden M. (2014)[25], Liposomes for ultrasound-triggered drug delivery.

(Top) Liposomes contain an aqueous core and phospholipid bilayer membrane with a hydrophobic bilayer to accommodate drugs such as doxorubicin (Bottom) Focused ultrasound can be used to increase the fluid temperature within the focus to alter membrane permeability and trigger drug release from temperature-sensitive liposomes.

1.3.1.1 Limitations

Whilst the heating effect being contained within the ultrasound focus (~ a few cm) is essential to ensuring minimal off-target effects, in practice, this also makes it less efficient at targeting larger organs. To achieve the desired therapeutic effect, multiple passes of the ultrasound transducer may be required[26,27]. As a result, it becomes difficult to ensure a uniform temperature distribution in larger treatment sites, devices or implants of interest which could cause uneven actuation and drug release from delivery vehicles.

1.3.2 Cavitation

Cavitation occurs when low frequency ultrasound interacts with bubbles in the medium. These bubbles can be endogenous, nucleated at interfaces or externally introduced as cavitations seeds. Depending on the mechanical index (MI) (**Fig. 5**), cavitation can be stable or unstable[28].

The mechanical index, MI is given by:

$$MI = \frac{P}{\sqrt{f}} \tag{5}$$

where P is the peak negative pressure in MPa and f is frequency of the ultrasound wave in MHz.

Stable cavitation occurs at lower MI where gas bubbles experience sustained oscillations at the ultrasound frequency. Inertial cavitation on the other hand is a transient phenomenon where the bubble forms, rapidly grows and collapses, releasing large energies into the fluid.

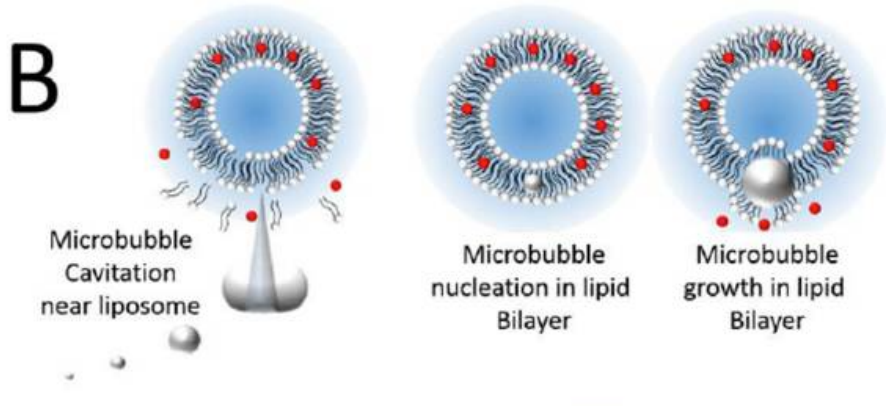

Figure 4 – Adapted and reproduced from Sirsi S. and Borden M. (2014)[25], using cavitation to control drug release from liposomes

Cavitation is one of the most common ways to trigger drug release and actuation in the body. In micelles and liposomes, cavitation results in bubbles nucleating and rapidly collapsing on the phospholipid shell to trigger drug release. The rate of delivery can be controlled by the ultrasound parameters; for instance, one can work within the stable cavitation regime to trigger slow controlled release, or conversely, utilize inertial cavitation to trigger rapid drug delivery.

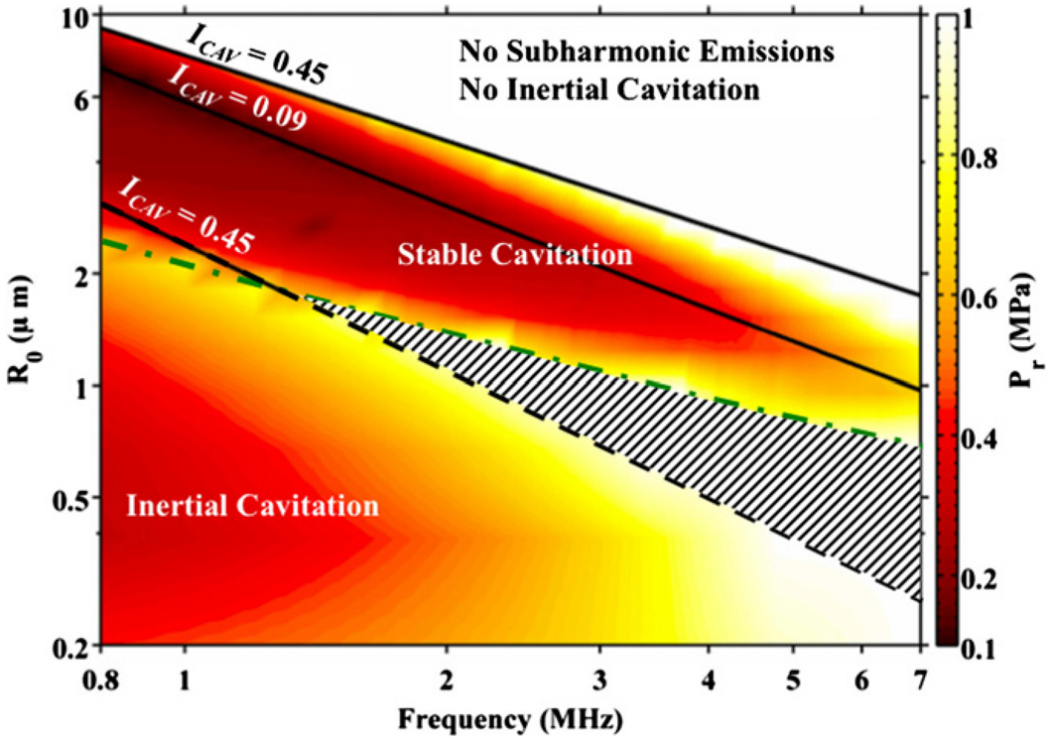

Figure 5 – Reproduced from Bader K.B. and Holland C.K. (2013)[28]

1.3.2.1 Limitations

The high mechanical effects associated with inertial cavitation may be useful in strategically detonating diseased or therapeutic cells[29] and unwanted masses such as kidney stones[1] and tumors. However, there are potentially short and long-term side effects[30] as a result of this therapy such as burns, and complications arising from exposure to radical byproducts. In fact, the FDA has instituted an MI ceiling of 1.9[31] to minimize potential health risks.

1.3.3 Acoustic Radiation Force

Acoustic radiation force (ARF) involves the transfer of momentum from the ultrasound waves to the (often) fluid particles because of attenuation or reflection. This results in the formation of localized fluid flow called acoustic streaming which can be harnessed to actuate mechanosensitive objects in the body. Although less common in biological systems and *in vivo* applications, the use of standing waves can result in the formation of pressure nodes and antinodes that attract or repel particles depending on their acoustic contrast factor.

The acoustic contrast factor is calculated by:

$$\phi = \frac{1}{3}\left[\frac{5\rho_p - 2\rho_0}{2\rho_p + \rho_0} - \frac{\beta_p}{\beta_0}\right] \quad (6)$$

where ρ_p and ρ_0 are the density of particle and fluid, respectively, β_p and β_0 compressibility of the particle and fluid, respectively. Particles with a positive acoustic contrast factor (e.g. polystyrene) will migrate to the pressure nodes and vice-versa.

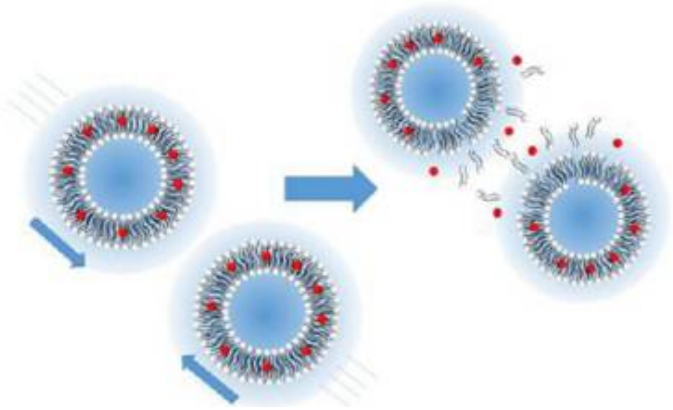

Figure 6 – Adapted and reproduced from Sirsi S. and Borden M. (2014)[25], Streaming effects from ARF are used to exert shear on the lipid bilayer

Acoustic streaming can be used to initiate drug release events by utilizing local flows to exert shear on the liposome surface. This causes disruption to the phospholipid bilayer which initiates the drug release event (**Fig. 6**). Standing waves on the other hand are not commonly used directly in the actuation mechanism for drug delivery, although they can supplement it. By generating anti-nodes, ARF (in combination with cavitation) can be used to guide microbubbles near tight junctions to assist with drug extravasation[32]. Finally, it is worth mentioning that ARF can be used in the biofabrication and patterning[33] of delivery vehicles for controlled-release applications.

1.3.3.1 Limitations

Currently there are limited opportunities to utilize ARF as an actuation mechanism for rigid or semi-rigid bodies such as those used as vehicles for drug delivery. However, there is promising research being done on mechanophores[34]. If we can tune these chemical moieties to respond to piconewton forces exerted by ARF, it can then be used as another mechanism to couple ultrasound with mechanical actuation on macroscopic delivery vehicles.

1.4 Contrast Agents and Sonosensitizers

Contrast agents and sonosensitizers are usually nano to micrometer-sized particles with a different acoustic impedance from its surroundings. These particles are exploited to selectively label a region of interest, with the former used to enhance ultrasound contrast and the latter to increase the actuation effects from ultrasound. Most contrast agents are sonosensitizers and vice-versa, and they only differ by the role that they are assigned to when placed in a system. Smart drug delivery systems can benefit from improvements in both imaging and actuation parameters; however, apart from good echogenicity, they need to be biocompatible and allow stable deployment in most materials used for delivery vehicles. Some of these commonly used particles will be discussed below.

1.4.1 Microbubbles

Microbubbles are 1 – 3 μm sized bubbles stabilized by a thin shell of protein, polymer of phospholipids. They have seen use as both contrast agents[35] and sonosensitizers[36], with notable studies like the vascular imaging of the brain[37] being performed with their assistance. They are also frequently used as drug carriers[38] albeit with low loading efficiency. Microbubbles are also stable only on the order of a few days[39] and their soft shells make it difficult to incorporate them in bulk materials. Due to their relatively large size, microbubbles are also not likely to be chosen to manipulate polymer or hydrogel nano and microarchitectures.

1.4.2 Metal and Inorganic Particles

Unlike microbubbles, metal and inorganic particles are typically denser and stiffer than soft tissue, allowing them to act as contrast agents and sonosensitizers. Whilst they are rarely used in vivo as contrast agents[40] due to their biotoxicity and poor renal clearance, particles such as silicone[41–43], tungsten[44] and hydroxyapatite[24] are commonly used as sonosensitizers within bulk materials to enhance viscous dissipation and cavitation effects, that trigger deformations in the material matrix to manipulate drug release. Overall, these particles are likely going to continue to be incorporated in drug delivery vehicles but more studies may

need to be done to make them more biocompatible, such as via PEGylation[45], to make them more compatible with certain therapeutics.

1.4.3 Gas Vesicles

Gas vesicles (GVs), are cylindrical, cone-tipped shaped proteins derived from buoyant microbes, which possess 2 nm thick protein shells enclosing air-filled compartments with dimensions on the order of 200 nm[12]. These hollow protein nanostructures are stable at physiologically relevant conditions by allowing air to partition across the shell interface whilst preventing the transport of water and solute particles. In its intact state, GVs effectively scatter sound waves and serve as ultrasound contrast agents that are currently being utilized in many *in vivo* applications to control and image biological function[11,13,46]. Genetically encoded GVs have also been used as sonosensitizers in cells[29], but have yet to be incorporated in synthetic materials. Due to its size, biocompatibility, and structural strength, GVs have the potential to be used as imaging and actuation ultrasound enhancers for biomaterials and micromachines used for smart drug delivery.

1.5 References

1.Pishchalnikov, Y. A. *et al.* Cavitation Bubble Cluster Activity in the Breakage of Kidney Stones by Lithotripter Shock Waves. *J. Endourol. Endourol. Soc.* **17**, 435–446 (2003).

2.Szabo, T. L. Chapter 3 - Acoustic Wave Propagation. in *Diagnostic Ultrasound Imaging: Inside Out (Second Edition)* (ed. Szabo, T. L.) 55–80 (Academic Press, 2014). doi:10.1016/B978-0-12-396487-8.00003-3.

3.Dukhin, A. S. & Goetz, P. J. Chapter 3 - Fundamentals of Acoustics in Homogeneous Liquids: Longitudinal Rheology. in *Studies in Interface Science* (eds. Dukhin, A. S. & Goetz, P. J.) vol. 24 91–125 (Elsevier, 2010).

4.Ng, A. & Swanevelder, J. Resolution in ultrasound imaging. *Contin. Educ. Anaesth. Crit. Care Pain* **11**, 186–192 (2011).

5.Maresca, D. *et al.* Biomolecular Ultrasound and Sonogenetics. *Annu. Rev. Chem. Biomol. Eng.* **9**, 229–252 (2018).

6.Yusefi, H. & Helfield, B. Ultrasound Contrast Imaging: Fundamentals and Emerging Technology. *Front. Phys.* **10**, (2022).

7.Unnikrishnan, S. & Klibanov, A. L. Microbubbles as ultrasound contrast agents for molecular imaging: preparation and application. *AJR Am. J. Roentgenol.* **199**, 292–299 (2012).

8.Paefgen, V., Doleschel, D. & Kiessling, F. Evolution of contrast agents for ultrasound imaging and ultrasound-mediated drug delivery. *Front. Pharmacol.* **6**, 197 (2015).

9.Ferrara, K., Pollard, R. & Borden, M. Ultrasound Microbubble Contrast Agents: Fundamentals and Application to Gene and Drug Delivery. *Annu. Rev. Biomed. Eng.* **9**, 415–447 (2007).

10.Fu, L. & Ke, H.-T. Nanomaterials incorporated ultrasound contrast agents for cancer theranostics. *Cancer Biol. Med.* **13**, 313–324 (2016).

11.Shapiro, M. G. *et al.* Biogenic gas nanostructures as ultrasonic molecular reporters. *Nat. Nanotechnol.* **9**, 311–316 (2014).

12.Lakshmanan, A. *et al.* Preparation of biogenic gas vesicle nanostructures for use as contrast agents for ultrasound and MRI. *Nat. Protoc.* **12**, 2050–2080 (2017).

13.Bourdeau, R. W. *et al.* Acoustic reporter genes for noninvasive imaging of microorganisms in mammalian hosts. *Nature* **553**, 86–90 (2018).

14.Sarvazyan, A. P., Rudenko, O. V. & Nyborg, W. L. Biomedical applications of radiation force of ultrasound: historical roots and physical basis. *Ultrasound Med. Biol.* **36**, 1379–1394 (2010).

15.Shankar, H. & Pagel, P. S. Potential adverse ultrasound-related biological effects: a critical review. *Anesthesiology* **115**, 1109–1124 (2011).

16.Wang, Y., Wang, Z.-B. & Xu, Y.-H. Efficacy, Efficiency, and Safety of Magnetic Resonance-Guided High-Intensity Focused Ultrasound for Ablation of Uterine Fibroids: Comparison with Ultrasound-Guided Method. *Korean J. Radiol.* **19**, 724–732 (2018).

17.Stewart, E. A. *et al.* The Comparing Options for Management: PAtient-centered REsults for Uterine Fibroids (COMPARE-UF) registry: rationale and design. *Am. J. Obstet. Gynecol.* **219**, 95.e1-95.e10 (2018).

18.Linares-Espinós, E. *et al.* New technologies and techniques for prostate cancer focal therapy. *Minerva Urol. E Nefrol. Ital. J. Urol. Nephrol.* **70**, 252–263 (2018).

19.Merckel, L. G. *et al.* First clinical experience with a dedicated MRI-guided high-intensity focused ultrasound system for breast cancer ablation. *Eur. Radiol.* **26**, 4037–4046 (2016).

20.Aubry, J.-F. *et al.* The road to clinical use of high-intensity focused ultrasound for liver cancer: technical and clinical consensus. *J. Ther. Ultrasound* **1**, 13 (2013).

21.Needham, D., Anyarambhatla, G., Kong, G. & Dewhirst, M. W. A new temperature-sensitive liposome for use with mild hyperthermia: characterization and testing in a human tumor xenograft model. *Cancer Res.* **60**, 1197–1201 (2000).

22.Weinstein, J. N., Magin, R. L., Yatvin, M. B. & Zaharko, D. S. Liposomes and local hyperthermia: selective delivery of methotrexate to heated tumors. *Science* **204**, 188–191 (1979).

23.Tacker, J. R. & Anderson, R. U. Delivery of antitumor drug to bladder cancer by use of phase transition liposomes and hyperthermia. *J. Urol.* **127**, 1211–1214 (1982).

24.Levingstone, T., Ali, B., Kearney, C. & Dunne, N. Hydroxyapatite sonosensitization of ultrasound-triggered, thermally responsive hydrogels: An on-demand delivery system for bone repair applications. *J. Biomed. Mater. Res. B Appl. Biomater.* **109**, 1622–1633 (2021).

25.Sirsi, S. R. & Borden, M. A. State-of-the-art materials for ultrasound-triggered drug delivery. *Adv. Drug Deliv. Rev.* **72**, 3–14 (2014).

26.Tillander, M. *et al.* High intensity focused ultrasound induced in vivo large volume hyperthermia under 3D MRI temperature control. *Med. Phys.* **43**, 1539–1549 (2016).

27.Partanen, A. *et al.* Reduction of peak acoustic pressure and shaping of heated region by use of multifoci sonications in MR-guided high-intensity focused ultrasound mediated mild hyperthermia. *Med. Phys.* **40**, 013301 (2013).

28.Bader, K. B. & Holland, C. K. Gauging the likelihood of stable cavitation from ultrasound contrast agents. *Phys. Med. Biol.* **58**, 127–144 (2013).

29.Bar-Zion, A. *et al.* Acoustically triggered mechanotherapy using genetically encoded gas vesicles. *Nat. Nanotechnol.* **16**, 1403–1412 (2021).

30.Topaz, M. Possible Long-Term Complications in Ultrasound-Assisted Lipoplasty Induced by Sonoluminescence, Sonochemistry, and Thermal Effect. *Aesthet. Surg. J.* **18**, 19–24 (1998).

31.Şen, T., Tüfekçioğlu, O. & Koza, Y. Mechanical index. *Anatol. J. Cardiol.* **15**, 334–336 (2015).

32.Arvanitis, C. D., Bazan-Peregrino, M., Rifai, B., Seymour, L. W. & Coussios, C. C. Cavitation-enhanced extravasation for drug delivery. *Ultrasound Med. Biol.* **37**, 1838–1852 (2011).

33.Wu, D. *et al.* Biomolecular actuators for genetically selective acoustic manipulation of cells. *Sci. Adv.* **9**, eadd9186 (2023).

34.P. Kabb, C., S. O'Bryan, C., D. Morley, C., E. Angelini, T. & S. Sumerlin, B. Anthracene-based mechanophores for compression-activated fluorescence in polymeric networks. *Chem. Sci.* **10**, 7702–7708 (2019).

35.Frinking, P., Segers, T., Luan, Y. & Tranquart, F. Three Decades of Ultrasound Contrast Agents: A Review of the Past, Present and Future Improvements. *Ultrasound Med. Biol.* **46**, 892–908 (2020).

36.Sun, L. *et al.* Ultrasound Microbubbles Mediated Sonosensitizer and Antibody Co-delivery for Highly Efficient Synergistic Therapy on HER2-Positive Gastric Cancer. *ACS Appl. Mater. Interfaces* **14**, 452–463 (2022).

37.Errico, C. *et al.* Ultrafast ultrasound localization microscopy for deep super-resolution vascular imaging. *Nature* **527**, 499–502 (2015).

38.Lentacker, I., Geers, B., Demeester, J., De Smedt, S. C. & Sanders, N. N. Design and Evaluation of Doxorubicin-containing Microbubbles for Ultrasound-triggered Doxorubicin Delivery: Cytotoxicity and Mechanisms Involved. *Mol. Ther.* **18**, 101–108 (2010).

39.Feshitan, J. A., Chen, C. C., Kwan, J. J. & Borden, M. A. Microbubble size isolation by differential centrifugation. *J. Colloid Interface Sci.* **329**, 316–324 (2009).

40.Tan, Y., Chen, M., Chen, H., Wu, J. & Liu, J. Enhanced Ultrasound Contrast of Renal-Clearable Luminescent Gold Nanoparticles. *Angew. Chem. Int. Ed.* **60**, 11713–11717 (2021).

41.Osminkina, L. A. *et al.* Effects of Nanostructurized Silicon on Proliferation of Stem and Cancer Cell. *Bull. Exp. Biol. Med.* **151**, 79–83 (2011).

42.Osminkina, L. A. *et al.* Porous silicon nanoparticles as efficient sensitizers for sonodynamic therapy of cancer. *Microporous Mesoporous Mater.* **210**, 169–175 (2015).

43.Sviridov, A. P. *et al.* Porous silicon nanoparticles as sensitizers for ultrasonic hyperthermia. *Appl. Phys. Lett.* **103**, 193110 (2013).

44.Kubota, T., Kurashina, Y., Zhao, J., Ando, K. & Onoe, H. Ultrasound-triggered on-demand drug delivery using hydrogel microbeads with release enhancer. *Mater. Des.* **203**, 109580 (2021).

45.Suk, J. S., Xu, Q., Kim, N., Hanes, J. & Ensign, L. M. PEGylation as a strategy for improving nanoparticle-based drug and gene delivery. *Adv. Drug Deliv. Rev.* **99**, 28–51 (2016).

46.Lakshmanan, A. *et al.* Molecular Engineering of Acoustic Protein Nanostructures. *ACS Nano* **10**, 7314–7322 (2016).

47.Maresca, D., Sawyer, D. P., Renaud, G., Lee-Gosselin, A. & Shapiro, M. G. Nonlinear X-Wave Ultrasound Imaging of Acoustic Biomolecules. *Phys. Rev. X* **8**, 041002 (2018).

48.Maresca, D. *et al.* Nonlinear ultrasound imaging of nanoscale acoustic biomolecules. *Appl. Phys. Lett.* **110**, 073704 (2017).

Chapter II

ULTRASOUND CONTROLLED DRUG DELIVERY BY ACOUSTICALLY SWITCHABLE HYDROGELS

This chapter is in large part a reformatted version of the manuscript entitled "Ultrasound controlled drug delivery by acoustically switchable hydrogels (DASH)" by Abundo M.P., Tifrea A.T., Buss M.J., Barturen-Larrea P., Jin Z., Malounda D. and Shapiro M.G. currently in preparation.

2.1 Abstract

Devices that can be remote-controlled to precisely deliver biomedicines to sites of disease are a major goal of biomedical research. However, most existing externally triggered delivery systems are based on complex chemical architectures or miniaturized electromechanical devices that are controlled with light or electromagnetic signals, which require custom instrumentation and are respectively challenging to apply in deep tissues or have limited spatial precision. Here we present a drug delivery platform comprising a simple protein-containing hydrogel that can be both imaged and triggered to release drugs at specific locations using commonplace ultrasound imaging devices. We show that the addition of cylindrical air-filled protein nanostructures called gas vesicles (GVs) to hydrogels blocks the diffusion of drug payloads out of the gel and allows the gel to be visualized with ultrasound. An increase in ultrasound pressure causes the GVs to collapse when the gels reach a specific anatomical location, instantly converting these steric blockers into percolation channels, leading to a 71.5-fold increase in drug diffusion and rapid release from the gel. We evaluate this concept through *in vitro* measurements of ultrasound-modulated diffusion and drug release and targeted *in vivo* release in the lower gastrointestinal tract. Then we demonstrate the use of orally administered hydrogel particles to deliver etanercept in the duodenum to treat gastrointestinal inflammation in a rat model of colitis. Delivery by acoustically switchable hydrogels (DASH) enables local, image-guided drug delivery using a simple formulation and ubiquitously available ultrasound imaging equipment.

2.2 Introduction

The development of technologies for remote-controlled, targeted drug delivery represents a "holy grail" of biomedical research. When implemented successfully, these platforms allow therapeutics to reach specific anatomical locations in complex tissues such as the gastrointestinal (GI) tract, thereby maximizing efficacy at the intended site of action while minimizing side-effects. Ideally, remote-controlled drug delivery would be performed under image guidance, making it possible to monitor vehicle location, trigger release, and confirm payload delivery. However, executing these series of actions *in vivo* remains a challenge. Most existing approaches aiming to achieve this goal utilize complex micromachined devices triggered by electric[1] or magnetic fields[2,3], which are challenging to focus *in vivo*, or by light[4,5], which has limited penetration[6] in tissues. Moreover, these devices tend to not be biocompatible[7] and are expensive to produce, difficult to miniaturize and require dedicated external apparatus for monitoring and control[8,9].

If instead it were possible to develop a drug delivery vehicle that could be tracked and triggered with diagnostic ultrasound, this would enable image-guided drug delivery using ubiquitous, low-cost instruments. Moreover, if such vehicles could be manufactured via simple mixing of biocompatible components, this would enhance and accelerate their development and use in a wide range of clinical applications. Ultrasound is a particularly attractive modality for image-guided drug delivery due to its clinical ubiquity, deep penetration (order of 10 cm) and high resolution (order of 100 μm)[10].

Here we introduce a new class of hydrogel materials with ultrasound-controlled porosity and use these materials as vehicles to deliver protein therapeutics to a specific segment of the gastrointestinal tract. Delivery via acoustically switchable hydrogels (DASH) is enabled by adding cylindrical air-filled protein nanostructures called gas vesicles[11] (GVs) to hydrogels to block the diffusion of drug payloads out of the gel (**Fig. 1, a-b**). An increase in ultrasound pressure causes the GVs to collapse[12], instantly converting these steric blockers into percolation channels, leading to rapid drug diffusion and release (**Fig. 1c**). Because GVs also scatter ultrasound, they allow the location of the sonoporous vehicles to be visualized with

ultrasound imaging before activating release. Furthermore, the acoustic collapse of GVs eliminates the contrast[12–14], providing confirmation that release has been triggered (**Fig. 1d**).

In this study, we evaluate this concept through detailed measurements of ultrasound-modulated diffusion and drug release from DASH devices, then demonstrate their use to release proteins in the lower gastrointestinal tract following oral administration. Finally, we use this system to deliver etanercept to the duodenum of rats in a model of colitis, resulting in reduced inflammation and improvements in the disease activity index. The DASH platform enables local, image-guided drug delivery using a simple formulation and ubiquitously available ultrasound imaging equipment.

2.3 GV-containing hydrogels exhibit acoustically switchable biomolecular diffusivity

GVs are cone-tipped cylindrical nanostructures with diameters of ~85 nm and lengths of ~400 nm comprising a hollow air-filled interior enclosed by a 2 nm-thick protein shell (**Fig. 1a**). These nanostructures evolved as flotation devices in buoyant photosynthetic microbes, and can be harvested from such microbes with high yield and purity[15]. Over the last decade, GVs have been developed as ultrasound contrast agents[12], reporter genes[16], mechanical actuators[17], and cavitation seeds[18]. In their intact form, GVs scatter sound waves, enabling their imaging. When the ultrasound pressure exceeds a critical threshold (e.g., ~500 kPa), the GVs irreversibly collapse and loses approximately 97% (**Supplementary Data 1**) of their volume[19] (**Fig. 1, c-d**), with the air inside them dissolving in surrounding media.

Since the GV shell is impermeable to molecules other than gases, we hypothesized that the presence of GVs in a hydrogel would restrict the diffusion of other biomolecules contained in the gel. We focused on protein payloads because they represent one of the most potent and selective classes of therapeutics that are challenging to deliver due to their sensitivity to formulation and in vivo transit conditions. To test our hypothesis, we used confocal microscopy to track the diffusion of fluorescently labelled bovine serum albumin (BSA) through a composite GV and hydrogel "GV-gel" system. We polymerized GV-gels containing different volume fractions of *Anabaena flos-aquae* GVs and Acrylamide/Bis-acrylamide monomers inside glass capillaries and loaded an adjacent reservoir with a solution of BSA-AlexaFluor 647. Then, we recorded the evolution of fluorescence across the capillary length as a function of time[20] (**Fig. 1e**) and fitted the resulting fluorescence curves to a one-dimension diffusion equation to obtain the diffusion coefficient of BSA for each GV-gel configuration. From this, we were able to confirm that GVs inhibit BSA diffusion in the hydrogel matrix through the lower diffusion coefficients measured (**Fig. 1f, empty circles**).

To test the hypothesis that *in situ* collapse of the embedded GVs would result in enhanced diffusion within the hydrogel, we used a diagnostic ultrasound transducer to apply an ultrasound pressure greater than the GV critical collapse pressure to the GV-gels. This caused

the diffusion coefficient of BSA to increase to values at or above those measured in GV-free gels (**Fig. 1f, filled circles**). We found the dynamic range of diffusivities between the ultrasound "on" and "off" states to be optimal at a GV and polymer concentration of 15% and 10% by volume, respectively (**Fig. 1g**).

We hypothesized that this acoustically switchable behavior can be further widened by forming GV clusters prior to gelation. This increase in inter-GV connectivity and therefore, decrease in inter-GV distance, is expected to make diffusion around intact GVs more challenging while extending the percolation networks created by GV collapse. To test this hypothesis, we clustered GVs using biotin and streptavidin, generating aggregates with hydrodynamic diameters of around 1 μm (**Fig. 1h).** Embedding these in the hydrogel reduced diffusion in the presence of intact GV clusters (at a 15% volume fraction) by a factor of four compared to unclustered GVs, while doubling its diffusivity upon GV collapse (**Fig. 1i**). As a result, the clustered GV-gel showed an ultrasound-induced diffusivity fold-change of 71.5 ± 9.8 (*mean ± s.e.m., N = 5,* **Fig. 1j**). These experiments demonstrate the ability of GVs to impart common hydrogel materials with acoustically switchable porosity that affects protein diffusivity.

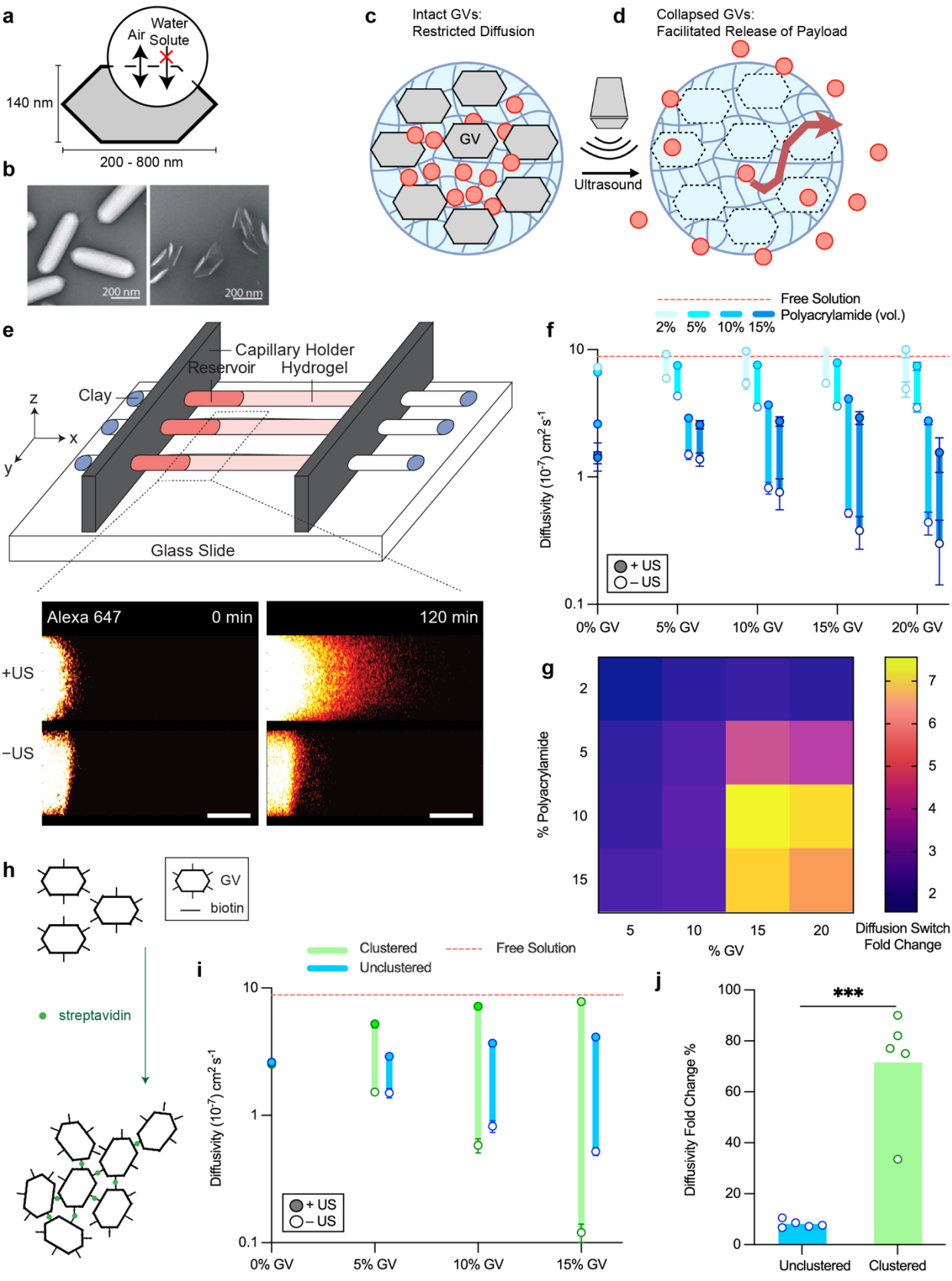
a
Water
Air
Solute
140 nm
200 - 800 nm
b
200 nm
200 nm
c
Intact GVs:
Restricted Diffusion
GV
d
Collapsed GVs:
Facilitated Release of Payload
Ultrasound
e
Capillary Holder
Reservoir
Hydrogel
Clay
z
x
y
Glass Slide
Alexa 647
0 min
120 min
+US
−US
f
Free Solution
Polyacrylamide (vol.)
2%
5%
10%
15%
Diffusivity (10^{-7}) $cm^2 s^{-1}$
10
1
0.1
+ US
− US
0% GV
5% GV
10% GV
15% GV
20% GV
g
% Polyacrylamide
2
5
10
15
5
10
15
20
% GV
7
6
5
4
3
2
Diffusion Switch
Fold Change
h
GV
biotin
streptavidin
i
Clustered
Unclustered
Free Solution
Diffusivity (10^{-7}) $cm^2 s^{-1}$
10
1
0.1
+ US
− US
0% GV
5% GV
10% GV
15% GV
j
***
Diffusivity Fold Change %
100
80
60
40
20
0
Unclustered
Clustered

Fig. 1 GV-gels produce ultrasound-modulated diffusivity changes. a, Schematic of a gas vesicle highlighting its ability to exclude volume from surrounding water and solute. **b,** TEM images showing intact (left) and ultrasound-induced collapsed (right) gas vesicles. **c,** GVs dispersed in a material act as diffusion steric blockers preventing the release of internally embedded payload. **d,** When the ultrasound pressure exceeds the GV critical collapse pressure, embedded GVs are shown to collapse and liberate excluded volume within the gel, triggering rapid outflow diffusion of payload. **e,** Illustration of the experimental set-up. GV-gels of varying compositions are polymerized within glass capillary tubes and loaded with a BSA-AlexaFluor 647 reservoir. It is then placed onto a glass slide mount for confocal imaging. **f,** Switch-like diffusivity changes of BSA-AlexaFluor through GV-gels with and without ultrasound exposure for varying GV and polyacrylamide volume fractions ($N = 5$, *mean* ± *s.e.m.*). **g,** Fold change in diffusion between the intact GV "ultrasound off" and collapsed GV "ultrasound on" states. **h,** Schematic of GV clustering reaction using biotin and streptavidin. **i,** Switch-like diffusivity changes of BSA-AlexaFluor through clustered and unclustered GV-gels with and without ultrasound exposure for 10% polyacrylamide and varying GV volume fractions ($N = 5$, *mean* ± *s.e.m.*). **j,** Clustering GVs produce a larger diffusivity dynamic range compared to unclustered GVs ($p = 0.0002$, $N = 5$).

2.4 DASH devices enable imaging and spatially targeted on-demand drug release in vitro

Having demonstrated switchable diffusivity, we set out to test the ability of DASH gels to release drug payloads on command. We formed prototype DASH devices by mixing the hydrogel reagents, clustered GV and the fluorescent BSA payload in 3D-printed cylindrical moulds with a diameter of 0.5 mm and a height of 2 mm (**Fig. 2a**). The gels were then preincubated in a solution of PBS for 2 hours to remove loosely bound BSA on or near the hydrogel surface (**SFig. 1**) and transferred into a stirred vial containing fresh buffer (**Fig. 2b**). We applied ultrasound to a subset of the gels and tracked the fluorescence intensity of the solution over 12 hours, finding that while gels without ultrasound exposure retained most of their payload, DASH devices actuated by ultrasound released most of their BSA within 2-3 hours, following near-linear release kinetics leading to nearly complete release after 5 hours (**Fig. 2c**). These results indicate the DASH gels can serve as ultrasound-triggered delivery vehicles.

Having determined the release kinetics of the DASH gels, we designed an experiment to demonstrate their ability to be imaged and actuated to release a payload in a spatially selective manner. We dispersed DASH devices in 1% agarose with inter-gel spacing of approximately 5 mm (**Fig. 2d**). We used a diagnostic ultrasound transducer operating at 6 MHz and 200 kPa peak positive pressure to locate and image the gels using xAM mode (**Fig. 2f**). We then selected several individual DASH gels (indicated by the dashed red circles in **Fig. 2e**) for actuation by increasing the ultrasound imaging voltage such that the applied pressure (550 kPa) would collapse their GVs, which is confirmed immediately by the disappearance of their ultrasound contrast (**Fig. 2g**). We observed that this acoustic switching of the gels resulted in selective payload release as shown by the diffusion of BSA into the agarose phantom (**Fig. 2h**). These results validate the capability of GV-gels to be used as ultrasound-guided delivery vehicles in vitro.

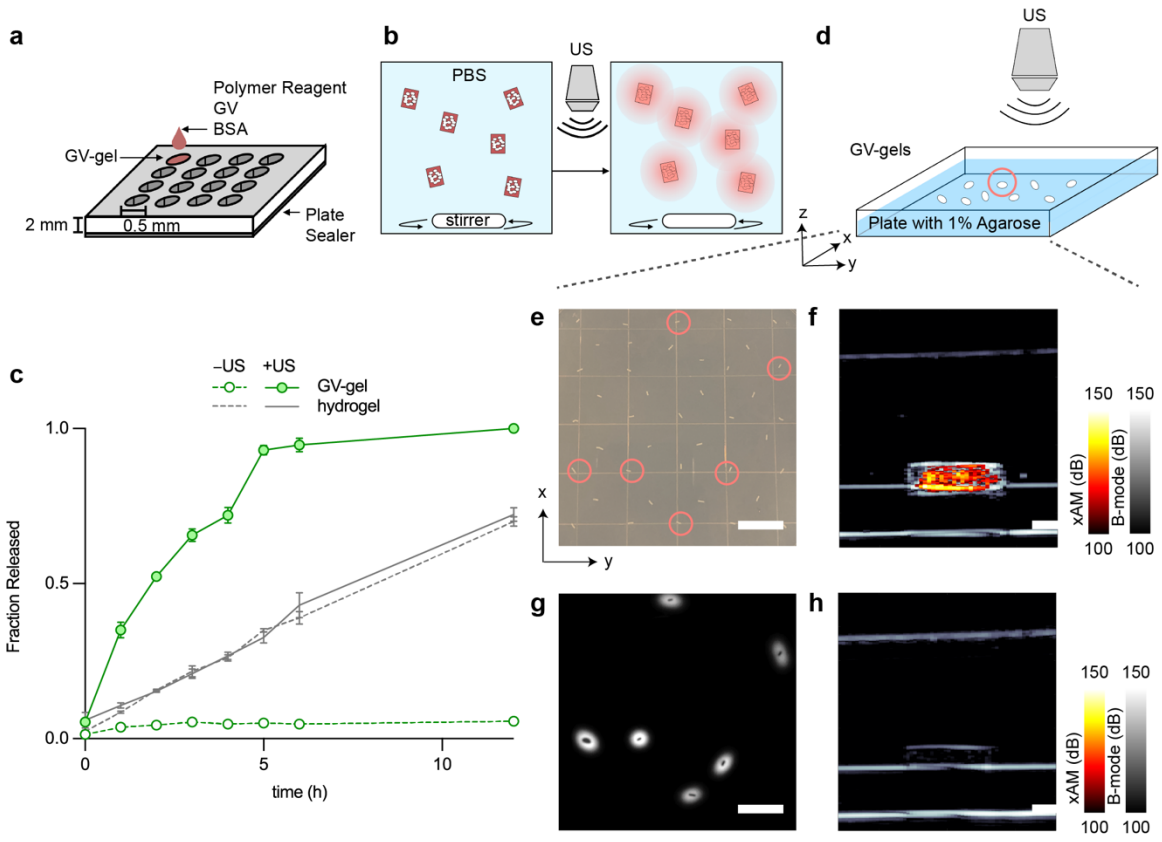

Fig. 2 DASH enables in vitro spatially targeted payload release with ultrasound-modulated release kinetics. a, Schematic of the 3D-printed mould used to form millimetre-sized cylinders. **b,** Diagram of experimental set-up used to track fluorescent payload release over time. GV-gels are placed into a vial containing simulated stomach fluid and stirred for 12 hours. The kinetics of payload release is monitored by aliquoting samples from the vial every hour and determining the fluorescence intensity. **c,** Release profiles of clustered GV-gels (green) with and without ultrasound exposure *(N* = 3, *mean* ± *s.e.m.*) compared to the no-GV hydrogel only controls (grey). Fraction released is defined as the fluorescence signal in the vessel normalized to the fluorescence signal at the end of the experiment. **d**, Diagram of the experimental setup used to assess spatial targeting performance of the drug delivery system *in vitro*. GV-gels are dispersed on a 1 %wt agarose phantom, and an ultrasound probe is used to target individual gels for collapse. **e,** Top-down photo of the plate showing dispersed GV-gels in agarose. GV-gels circled in red depict those selected for ultrasound targeting at t = 0. **f,** xAM image of GV-gels prior to ultrasound collapse. **g,** Fluorescence

subtraction image obtained between t = 12 hours post GV-collapse and at t = 0. **h,** xAM image of GV-gels post ultrasound collapse.

2.5 DASH gels enable spatially selective ultrasound-triggered drug release in vivo

One of the most immediate applications of spatially triggered drug delivery devices is the gastrointestinal tract, due to a range of GI pathologies requiring local treatment and the desire to use oral routes of administration for drugs designed to act elsewhere in the body. Thus, we chose the GI tract as the initial proving ground for DASH. To demonstrate the spatiotemporal control of drug release in vivo, we orally gavaged a suspension containing BSA-loaded DASH gels in PBS into Sprague Dawley rats (**Fig. 3a**). After 5 hours, an ultrasound probe was used to locate GV-gels in the cecum (**Fig. 3b**) and a high pressure of (550 kPa) was applied to trigger protein release (**Fig. 3c**). The large intestine of the rats were collected and plated individually in PBS. Similar to existing fluorescence-based methods used to measure gastrointestinal permeability[21] and gut transit[22], the intestines were gently flushed with PBS after 12 hours to collect gut contents and solid debris including DASH gels, leaving behind only proteins (and attached fluorophores) that were released from the gels and absorbed by intestinal walls. Fluorescence images of the GI tract taken 12 hours after triggered release (**Fig. 3d**) showed significant signal localized in the proximal colon at 12 hours only in rats that received a collapsing ultrasound pulse (**Fig. 3e**). These results show that DASH gels can be imaged and triggered noninvasively with ultrasound inside intact living animals, leading to localized release of a protein payload.

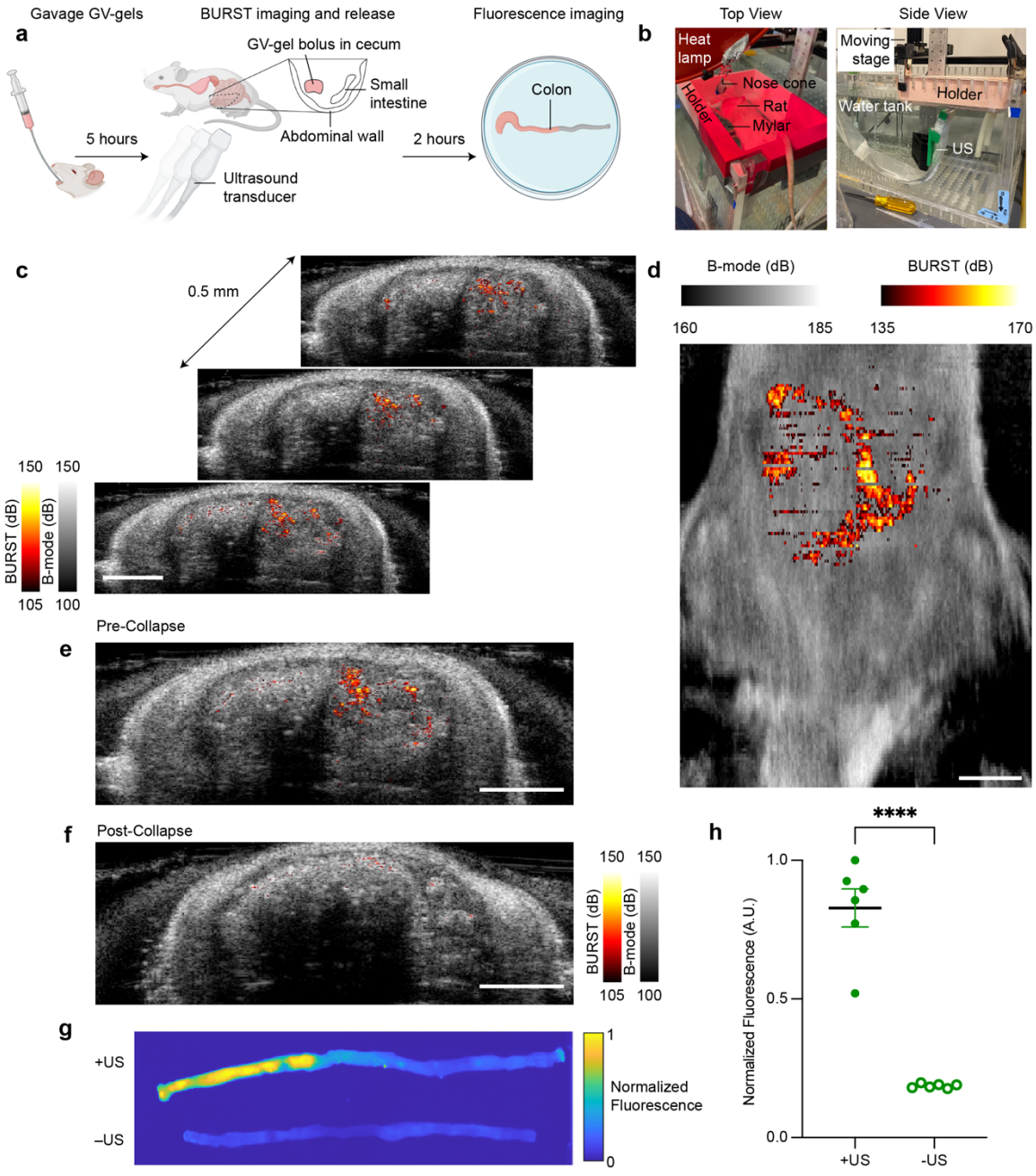
a
Gavage GV-gels
BURST imaging and release
Fluorescence imaging
GV-gel bolus in cecum
Small intestine
Abdominal wall
Ultrasound transducer
5 hours
2 hours
Colon
b
Top View
Side View
Heat lamp
Nose cone
Rat
Mylar
Holder
Moving stage
Holder
Water tank
US
c
0.5 mm
150 150
BURST (dB)
B-mode (dB)
105 100
d
B-mode (dB)
BURST (dB)
160 185
135 170
e
Pre-Collapse
f
Post-Collapse
150 150
BURST (dB)
B-mode (dB)
105 100
g
+US
–US
1
Normalized Fluorescence
0
h
****
Normalized Fluorescence (A.U.)
1.0
0.5
0.0
+US
-US

Fig. 3 In vivo spatially targeted imaging and payload release from GV-gels a, Illustration of the spatially targeted in vivo imaging and release experiment. **b,** Top and side view of the experimental setup used to hold the rat in place to carry out imaging and ultrasound triggered release. **c,** Representative stack of BURST images (heat color map) of the lower abdomen area overlaid on top of the anatomical B-mode images (grayscale) in the frontal-view plane five hours post-gavage. BURST signal was not observed in rats that were given saline gavage (**Supplementary Data 2**). **d,** 2D projection in the transverse plane of the composite BURST signals (heat color map) found in the gastrointestinal region overlaid on top of the anatomical B-mode images (grayscale). The composite BURST signal is calculated based on the mean intensity of manually drawn ROIs around gastrointestinal organs. Scale bars, 10 mm **e,** Ultrasound images of the cecum pre-collapse with xAM (heat color map) and B-mode (grayscale). Scale bars, 10 mm. **f,** Ultrasound images of the cecum post-collapse with xAM (heat color map) and B-mode (grayscale). Scale bars, 10 mm. **g,** Representative fluorescence in the rat colon with and without high pressure ultrasound GV-gel collapse. **h,** Statistical analysis of the retained fluorescence signal in the intestines between rats with and without high pressure ultrasound GV-gel collapse. $P < 0.0001$

2.6 DASH release of etanercept enables the treatment of colitis in animal model

Having shown that DASH can provide ultrasound-mediated targeted release of proteins *in vitro* and *in vivo*, we set out to apply it to the delivery of a protein therapeutic in a preclinical disease model. Intestinal bowel disease like ulcerative colitis (UC), affects 3.1 million[23] Americans. It is chronic and requires lifelong treatment and pain management as patients typically experience poor quality of life due to frequent episodes of relapse characterized by moderate to severe lesions in the large intestine. On a yearly average, adults with IBD are 21.8% more likely to visit healthcare providers four or more times and are 10.4% more likely to undergo surgery[23]. Among other treatments, colitis is treated with biologics inhibiting the pro-inflammatory cytokine tumor necrosis factor (TNF)[24]. These are administered systemically, often requiring higher doses to overcome clearance by the systemic circulation before reaching the inflammation site in the gut. Despite its effectiveness, this delivery method can expose patients to higher risks of dose-dependent side-effects such as infections and tumorigenesis due to systemic immunosuppression[25–27]. If anti-TNF agents could be delivered more directly to the colon, this could increase their dose at the target site while mitigating their systemic side-effects. We hypothesized that the DASH platform would allow us to deliver the monoclonal anti-TNF-α antibody, etanercept, to the colon and thereby treat colitis in a rat model of the disease. Etanercept is an FDA-approved treatment for autoimmune diseases in humans and has previously been validated to treat experimental colitis in rodents, where it was used due to its ability to react with the rat TNF-α[28–30].

To formulate DASH devices for etanercept, we incorporated the drug and GVs in a calcium alginate hydrogel, which has previously been validated for sustained release of monoclonal antibodies[31]. To protect the gels from stomach pH and enzymes, we dip-coated them with the enteric coating Eudragit FL30D55 (**Fig. 4a**). We then verified the ultrasound-mediated drug release kinetics of this system in simulated rat gastric fluid (**Fig. 4b**).

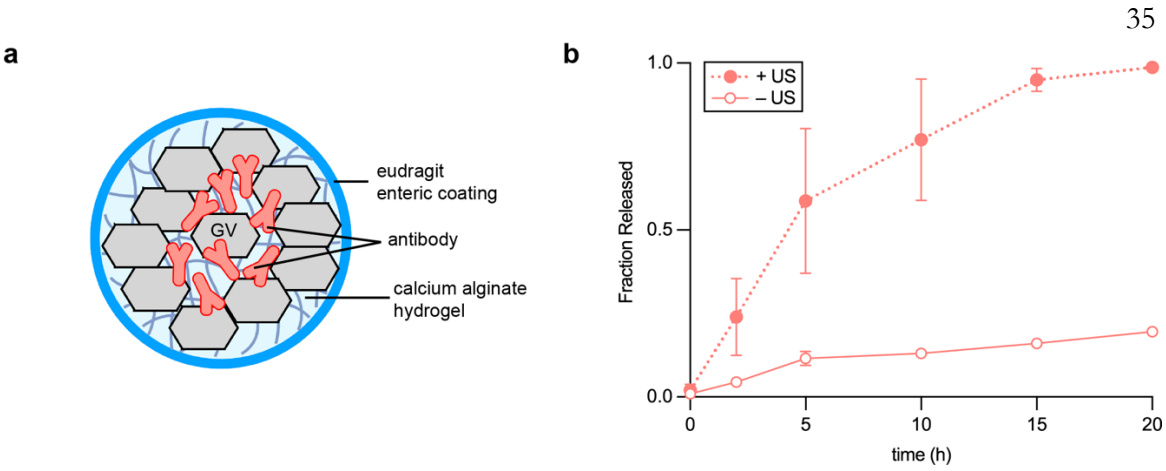

Fig. 4 GV-gels for oral delivery of biomolecules. a, Illustration of antibody loaded GV-gel based on calcium alginate. GV-gels for oral gavage in rodents are coated with a thin enteric coating layer of Eudragit. **b,** Ultrasound-mediated controlled release kinetics of BSA-AlexaFluor 647 from modified GV-gels.

We induced severe colitis in Sprague-Dawley rats by adding 4% dextran sulfate sodium (DSS) to the drinking water for five days. DSS-treated rats had a slower rate of weight gain relative to the healthy controls (**Supplementary Data 3**). We then treated the animals with daily oral gavage of a suspension of DASH-etanercept at a dose of 12.5 mg/rat-day (**Supplementary Data 4**) from days 6 to 11. Since most gels reach the cecum 5 hours after gavage, we triggered etanercept release by applying a high pressure (550 kPa) ultrasound pulse to the abdominal area (**Fig. 5a**) for animals in the treatment group. All rats were sacrificed at day 12 for blinded histopathological analysis of the colon by a nonaffiliated pathologist. Onset of severe colitis occurred on day 4 and can be described by a sudden decrease in the rate weight gain relative to the healthy controls[32] (**Fig. 5b**), an increase in disease activity index (DAI) (**Fig. 5c**), colonic tissue damage and colon shortening.

In DASH-etanercept treated rats, we observed a statistically significant recovery of the weight gain rates (**Fig. 5b**) and a reversal of the DAI (**Fig. 5c**), colon shortening (**Fig. 5e**) and colonic tissue damage trends (**Fig. 5d**). Post-mortem histological examination revealed that the treatment group had mild to no histological alterations due to colitis by the end of the treatment, with the regular structure of the lamina propria restored and comparable to those in the healthy rat controls. In contrast, rats that were given the DASH gels without ultrasound actuation and rats in the untreated control group demonstrated crypt abnormalities and inflammatory acute infiltration of the sub-epithelieum and lamina propria (**Fig. 5f**). Together, these results highlight the potential of DASH in the targeted oral delivery of antibodies for the treatment of chronic colitis.

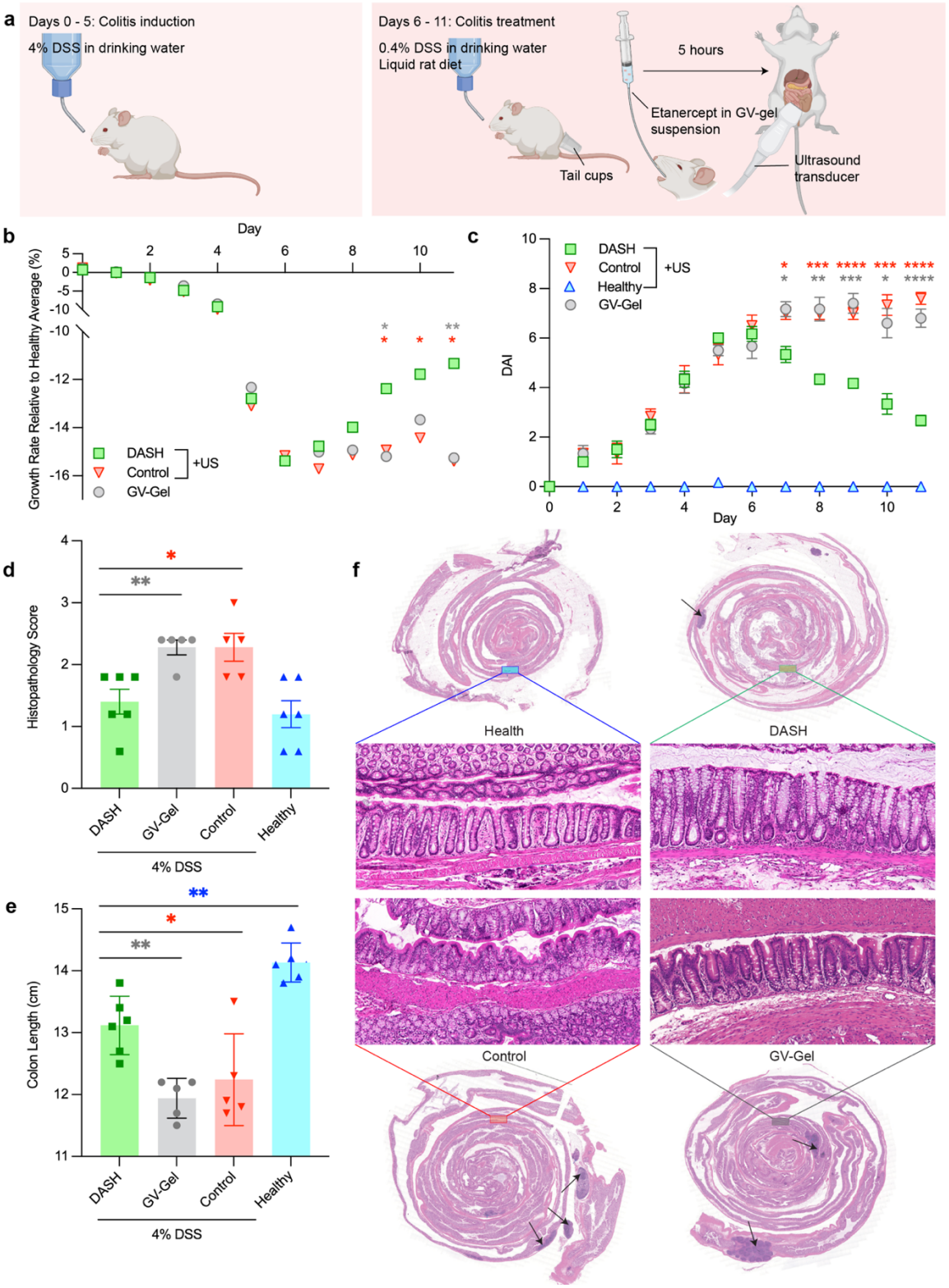
a
Days 0 - 5: Colitis induction
4% DSS in drinking water
Days 6 - 11: Colitis treatment
0.4% DSS in drinking water
Liquid rat diet
5 hours
Etanercept in GV-gel suspension
Tail cups
Ultrasound transducer
b
Day
Growth Rate Relative to Healthy Average (%)
DASH
Control
GV-Gel
+US
c
DAI
Day
DASH
Control
Healthy
GV-Gel
+US
d
Histopathology Score
DASH
GV-Gel
Control
Healthy
4% DSS
e
Colon Length (cm)
DASH
GV-Gel
Control
Healthy
4% DSS
f
Health
DASH
Control
GV-Gel

Fig. 5 GV-gels for the treatment of colitis in Sprague-Dawley rats using etanercept. **a,** Experimental workflow used to demonstrate treatment of colitis in rats using the GV-gel delivery vehicles. **b,** Percent changes in rat weight gain rate relative to healthy controls over the treatment period for rats with severe colitis that were given no treatment, GV-gel treatment (without ultrasound) and DASH treatment. Where not seen, error bars (± *s.e.m.*) are smaller than the symbol. The P-values for the statistically significant points during the treatment period are as follows for (i) DASH vs GV-gel: Day 9, $P = 0.0343$; Day 11, $P = 0.0004$ (ii) DASH vs control: Day 9, $P = 0.01783$; Day 10, $P = 0.0035$; Day 11, $P = 0.0010$. **c,** Changes in DAI for 11 days, which is the sum of the stool consistency index (0–3), faecal bleeding index (0–3) and weight loss index (0–4). The P-values for the statistically significant points during the treatment period are as follows for (i) DASH vs GV-gel: Day 7, $P = 0.0023$; Day 8, $P = 0.0003$; Day 9, $P = 0.00002$; Day 10, $P = 0.0013$; Day 11, $P < 0.00001$ (ii) DASH vs control: Day 7, $P = 0.0027$; Day 8, $P = 0.00001$; Day 9, $P < 0.00001$; Day 10, $P = 0.000053$; Day 11, $P < 0.00001$. **d,** Histopathology scores for rats in (b) and a no-DSS health control group. The P-values are (vs DASH) (i) GV-gels: $P = 0.0060$ (ii) control: $P = 0.0166$. **e,** Colon lengths of rats after the indicated treatments. The P-values are (vs DASH) (i) GV-gels: $P = 0.0011$ (ii) control: $P = 0.0405$ (iii) healthy: $P = 0.0013$ **f,** Representative H&E-stains of the colonic sections of different rat groups after the indicated treatment. Black arrows are pathologist-identified abscessed regions.

2.7 Discussion

Our work establishes DASH as a unique approach to targeted drug delivery that allows ubiquitous diagnostic ultrasound devices to trigger the release of therapeutic payloads spatially and temporally inside the body. DASH leverages the ability of GVs to simultaneously act as ultrasound contrast agents and collapsible steric blockers, allowing simple hydrogels to be both visualized and actuated with ultrasound. DASH devices are engineered to minimize payload leakage until actuated, and conversely, provide rapid release upon being triggered at the intended site of action. Spatiotemporal targeting is achieved by tracking the vehicle location using the ultrasound contrast generated by the GVs.

In this study, we established the fundamental concept of acoustically switchable hydrogel permeability, demonstrated its performance in triggered release of biomolecular payloads, and showed how this technology can be exploited to develop a targeted oral antibody delivery system to treat colitis. In future studies, the DASH technology can be extended to a wider range of cargoes[33] – from small-molecule drugs (~ 1 nm) to viruses such as adeno-associated virus (>20 nm) – by tuning the hydrogel mesh size relative to the hydrodynamic radius of the payload. These payloads could be released in contexts ranging from ingestible pills to implantable and interventional medical devices or smart robots navigating through a tissue[34]. In addition, using a combination of GV types with varying collapse pressures [35]can be used to sequentially release multiple payloads. Furthermore, acoustophoresis can be used to pattern GVs within the material[17] to create local variations in switchable diffusivity that could further enhance switchable release or facilitate multiplexing.

As with any new technology, further work is needed to optimize the DASH system and enable its broadest range of clinical applications. Depending on the therapeutic payload, it may be necessary to use hydrogels other than the polyacrylamide and alginate used in this study and establish compatibility with GVs as collapsible steric blockers. Additionally, for repeated chronic administration of GV-containing hydrogels, it will be important to characterize the immune accessibility and potential immunogenicity of the non-human GV proteins. Furthermore, for patients to be able to use DASH technology at home, consideration

must be given to ultrasound devices, including adhesive ultrasound devices[36–39] and machine learning algorithms to automatically recognize and trigger delivery vehicles at specific anatomical sites. For uses in the GI tract, it may also be necessary to deal with confounding gas and solid contents in ultrasound images. This task will be aided by GV-specific ultrasound pulse sequences[13,40–42] and patient preparation such as low-fiber diets, and in acute cases laxatives commonly prescribed prior to colonoscopy procedures.

Notwithstanding the need for further research, the relative simplicity and versatility of the DASH approach and its compatibility with existing FDA-approved hydrogel materials, drugs and ultrasound devices, makes this technology poised to dash toward exciting clinical applications.

2.8 Methods

Animals. 5-week-old male Sprague Dawley rats weighing between 150-160g were purchased from Charles River (USA). The rats were housed in the animal facility of the Office of Laboratory Animal Resources (OLAR) at the California Institute of Technology with a 13h/11h light/dark cycle with cage conditions kept between 22 to 24°C and 30 to 70% humidity. The rats were monitored daily for overall well-being and given ad libitum access to water and standard laboratory chow. All animals were acclimated for three days prior to performing experiments that are in accordance with an approved Institutional Animal Care and Use Committee (IACUC) protocol (IA15-1735).

Preparation of gas vesicles. Purified GVs from *Anabaena flos-aquae* with GvpC removed (AnaΔC) and subsequently, clustered to form larger aggregates were prepared as previously described[12,15].

Diffusion characterization. 50 µl of hydrogel reaction mixture is made by copolymerizing a predetermined volume fraction of acrylamide and bis-acrylamide (A7168: Sigma Aldrich) in prefiltered pH 7.4 phosphate buffered saline (PBS) solution at a fixed cross-linking density of 2.7%. 50 µl of purified *Anabaena Flos-Aquae* GVs solution was concentrated to a predetermined volume fraction (optical density, OD 24 = 1% vol. GV) and added to the hydrogel reaction mixture. The hydrogel reaction mixture is then degassed in a vacuum chamber for 30 min to rid the system of oxygen. 0.1 µl and 0.5 µl of initiators tetramethyl ethylene diamine (T9281: Sigma Aldrich) and 10% ammonium persulfate solution (A3678: Sigma Aldrich) respectively was then added to the reaction mixture and agitated slightly using a pipette to start the free-radical polymerization at room temperature (25ºC). Using the prepared syringe-capillary system, the hydrogel reaction mixture is immediately withdrawn into the glass capillary, leaving about a 1 inch of the glass capillary empty at the top for dye loading later. This recipe is expected to produce hydrogels of approximately 19 nm[43] pore sizes. The bottom of the glass capillary is quickly capped with some clay to prevent the hydrogel from drying or leaking out. To collapse the GVs in the GV-gel, the filled glass capillary is first placed into a PBS-filled container and held in place by solidified 1%

Agarose. An L10-4V 128-element linear array ultrasound transducer (Verasonics) operating at peak positive pressure of 600 kPa was then held in place over the capillary for 3 mins to collapse the GVs in the gel. GV collapse is verified visually from the loss of gel opacity, and from the loss of ultrasound signal within the gel. The capillary loaded gels are then equilibrated at room temperature with PBS for at least 6 hours prior to experiments.

Albumin from Bovine Serum (BSA) with AlexaFluor™ 647 conjugate (A34785: ThermoFisher Scientific) was diluted to 500 μg/ml using PBS and equilibrated at room temperature for 5 mins. A 1 ml BD Luer-Lok™ tip syringe fitted with a blunt 30G needle (SAI Infusion Technologies) was then used to inject the protein dye near the interface of the hydrogel casted within a 3-inch open-ended glass capillary (1B120-3: World Precision Instruments), ensuring all the air bubbles are extracted prior to experiments. Both ends of the capillary are then capped with clay to prevent evaporation. The experiments were then carried out as described[20] for rapid measurements of protein diffusion through hydrogels using a Zeiss LSM 800 inverted microscope fitted to a 2.5x objective lens (numerical aperture: 0.075). Fluorescence imaging was performed under an Alexa 647 channel (excitation: 587/25 nm, emission: 647/70 nm) and images were taken every 6 mins over a period of 2 hours.

The time series of fluorescence images from the capillary diffusivity experiments capillary were imported into MATLAB for image processing. The time evolution of the fluorescence intensity across the capillary length from the fluid-gel interface was recorded and averaged across the capillary cross-sectional area. Since the length of the gel (5 cm) is significantly larger that its diameter (0.6 mm) one can approximate the protein-dye transport in the gel to follow a 1-D diffusion model through an infinite slab given by the following equation:

$$F(x,t) = K\ erfc\left(\frac{x}{2\sqrt{D_{eff}\ t}}\right) \quad (1)$$

where K and D_{eff} are constants that represent the gel partitioning and diffusion coefficients of BSA respectively, F is the fluorescence intensity normalized to the dye reservoir intensity,

x is the distance from the interface and t is the time. The experimental data was then fitted to equation (1) using a nonlinear programming solver on MATLAB to obtain the two constants.

Acrylamide GV-gel preparation. The acrylamide GV-gel cargoes utilized the same hydrogel recipe as described in the BSA diffusivity experiments but with the addition of BSA-AlexaFluor 647 at a final dye concentration of 500 μg/ml also mixed into the polymerization precursor media. The reaction mixture was then pipetted into 0.4 μl cylindrical moulds and allowed to polymerize completely overnight in a humidified chamber to prevent drying out. Prior to experiment, the gels are incubated in PBS for 2 hours to remove loosely bound proteins. Collapse of GVs in the gel utilize the protocol described previously for diffusion characterization.

Calcium Alginate GV-gel preparation. Hydrogels were formed using solutions of 2 wt.% alginate (102877-746: VWR) in PBS solutions containing 15 vol.% clustered GVs, 25 mg/mL of etanercept (Y0001969: Sigma-Aldrich) reconstituted in bacteriostatic water as per supplier's guidelines, calcium carbonate ($CaCO_3$) (239216: Sigma-Aldrich) and D-Glucono-δ-lactone (GDL) (8.43794: Sigma-Aldrich). To make a homogenous gel, $CaCO_3$ was added to 2 mL of alginate solution to obtain a molarity of 144 mM and vortexed for 10s, and then left to degas at 37 °C overnight. 100 μL of the etanercept solution was then added to the mixture followed by GDL till it doubled the molarity of $CaCO_3$ to maintain a neutral pH. The resultant solution is gently mixed to prevent bubbles from being reintroduced and pipetted into 0.4 μl cylindrical moulds and allowed to polymerize completely overnight in a sealed humidified container within an incubator at 25 °C to prevent it from drying out and keep the hydrogels robust. Calcium alginate gels prepared using this method are expected to possess pore sizes of around 5 nm[44]. They are then incubated in PBS for 2 hours to remove loosely bound proteins. The gels were then enterically coated by lightly dip coating them in organic solutions of Eudragit FL30D55 (Evonik Industries) in acetone containing 3 vol.% ethanol and gently blasted with air to dry. The gels were then suspended in PBS prior to administration. This recipe makes enough therapeutic for 2 rats/day at a dose of around 12.5 mg/rat-day. To prepare for oral gavage, a 3 mL syringe was backfilled with 1 mL of PBS.

Using a second syringe, GV-gels are slowly withdrawn into the gavage needle. The gavage needle is then connected back to the first syringe.

In vitro release. 100 pieces of the acrylamide GV-gels were suspended in 30 ml fresh PBS and stirred at 37°C and 100 rpm. The experiment was performed in a dark room to minimize fluorophore photobleaching. Every 2 hours for a total of 12 hours, 10 μL of the suspension was aliquoted into a 90-well plate containing 100 μL of PBS. The wells were then analysed using a Spectramax M5 plate reader with the following wavelength settings: excitation: 587/25 nm and emission: 647/70 nm. After 72 hours, the suspension was aliquoted again to determine the total protein-dye payload present in all ten GV-gel cargoes. Fluorescence intensities collected during the time series were then normalised to the final intensity at 72 hours to determine the release kinetics of the GV-gel cargoes.

In vitro spatial targeting. Acrylamide GV-gels were evenly distributed and spaced at around 1 mm in a shallow petri dish filled with 1% agarose and allowed to set. An L10-4V 128-element linear array ultrasound transducer (Verasonics) was then operated at peak positive pressure of 200 kPa to image the gels, and subsequently at 600 kPa to trigger the release of fluorophores into the agarose for preselected GV-gels.

In vivo spatial targeting and release. Rats were fasted and given sucrose water, their abdomen hair shaved, and tail cups were placed 17 hours prior to experiments to minimize coprophagy. 1 mL acrylamide GV-gel suspension was orally gavaged into the rats. BURST imaging was then performed on the entirety of the rat abdomen 5 hours post-gavage to verify arrival of the GV-gel bolus in the cecum and subsequently trigger the release of fluorophores. The animals were then sacrificed, and the colon harvested and analyzed for fluorescence under a ChemiDoc.

DASH Treatment. During DASH treatment, the standard laboratory chow is replaced with rodent liquid diet (AIN-76, Bio-Serv) and custom fit tail cups are attached on each rat to prevent coprophagy to improve ultrasound imaging performance. Calcium alginate GV-gels loaded with etanercept as previously described were utilized in the DASH treatment and are freshly prepared prior to daily treatment. It is worth noting that etanercept or human Enbrel

is not an FDA approved treatment for colitis, but rather for rheumatoid arthritis[45]. However, we used it as it is a common human anti-TNF-α prescription with significant binding to rodent TNF-α without requiring a surrogate, unlike infliximab[46,47]. 1 mL of the hydrogel suspension was orally gavaged into the rats. 5 hours after administration, the rats are anesthetized and placed on a holder containing an ultrasound transparent window to enable imaging, verify GV-gel arrival in the cecum, and trigger GV collapse for etanercept release in the colon.

DSS-Induced Ulcerative Colitis Model. Severe ulcerative colitis was induced in rats allowing rats to consume 4% by weight of dextran sulfate sodium (36-50 kDa colitis-grade DSS, MP Biomedicals, USA) in their drinking water for five days. On day 6, DSS is reduced to 0.4% and DASH treatment is given once a day for six days until euthanized on day 11. During these 11 days, the rats were monitored daily for changes in weight and stool quality.

DAI. The DAI was scored using the following criteria: stool consistency (hard: 0, soft: 2, and diarrhea: 4), fecal occult blood using Hemoccult Sensa (Beckman Coulter) (negative: 0, positive: 2, and macroscopic: 4), and decrease in weight relative to the average weight of the healthy controls (less than 1%: 0, 1 to 5%: 1, 5 to 10%: 2, 10 to 20%: 3, and more than 20%: 4).

Histopathology and Scoring. Tissue samples of the colon were fixed in 3.7% paraformaldehyde overnight at 4°C, dehydrated in ethanol and embedded in paraffin. Haematoxylin and eosin (H&E) staining was then performed on the tissues for general histological observation. The histological scores were assessed in a blinded manner for inflammation severity (none: 0, slight: 1, moderate: 2, and severe: 3), polymorphonuclear neutrophil (PMN) infiltration/high power field (HPF) (less than 5: 0, 5 to 20: 1, 21 to 60: 2, 61 to 100: 3, and more than 100: 4), injury depth (none: 0, mucosa: 1, submucosa and mucosa: 2, and transmural: 3), crypt damage (none: 0, basal 1/3: 1, basal 2/3: 2, only surface epithelium intact: 3, and total crypt lost: 4), and adjustment to the tissue involvement multiplied by the percentage factor (0 to 25%: ×1, 26 to 50%: ×2, 51 to 75%: ×3, and 76 to

100%: ×4). The final score was then averaged across all indicators to determine disease severity.

2.9.1 Supplementary Data 1 – Volume change calculation

Supplementary Table 1 – GV dimensions (mean ± s.e.m.) measured using EM for use in volume estimations[15,48]. Intact GVs are assumed to be cylindrical in shape while collapsed GVs are assumed to be rectangular sheets with 1.8 nm wall thickness.

Intact *Anabaena flos-aquae* GV	
Length (nm)	519 ± 160
Width (nm)	85 ± 4
Collapsed *Anabaena flos-aquae* GV	
Length (nm)	519 ± 160
Width (nm)	89 ± 6
Estimated volume ratio (collapsed / intact)	0.028

2.9.2 Supplementary Data 2 – Negative Control for BURST Imaging

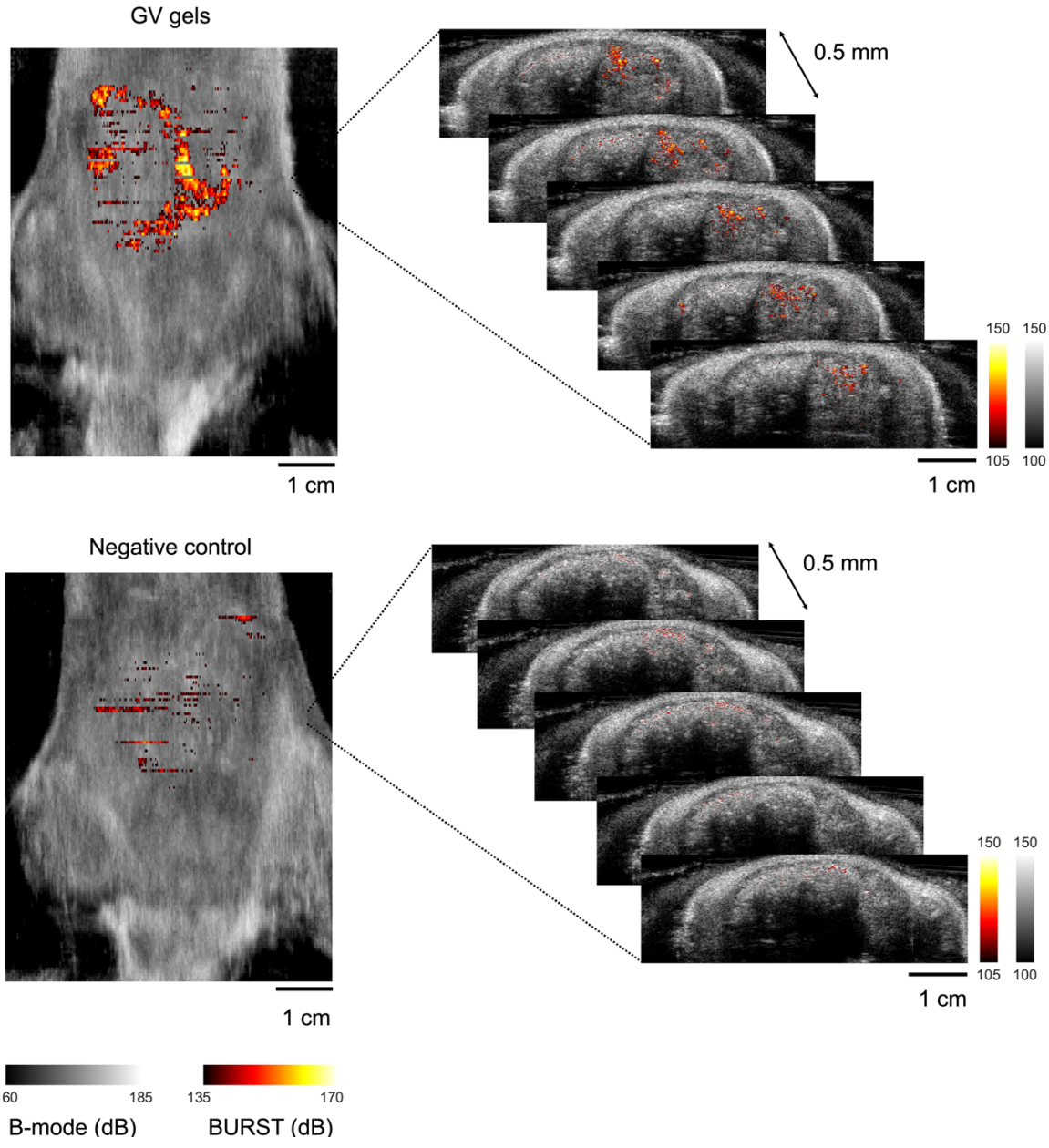

2.9.3 Supplementary Data 3 – Weight gain trends for healthy and colitis rats

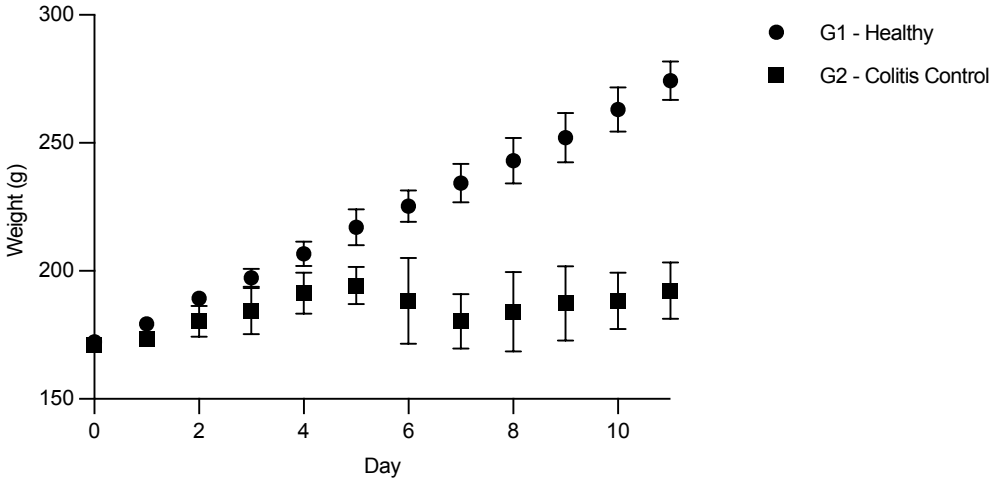

2.9.4 Supplementary Data 4 – Dosing experiment

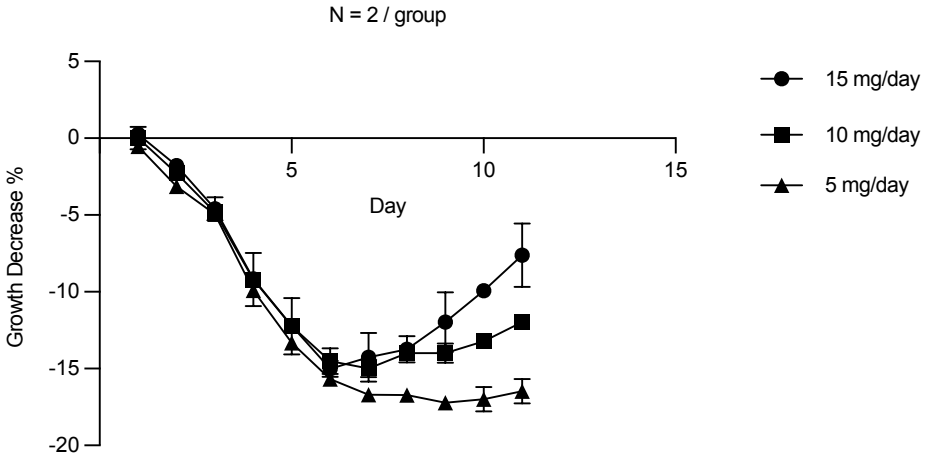

2.10 References

1.Svirskis, D., Travas-Sejdic, J., Rodgers, A. & Garg, S. Electrochemically controlled drug delivery based on intrinsically conducting polymers. *J. Controlled Release* **146**, 6–15 (2010).

2.Monge, M., Lee-Gosselin, A., Shapiro, M. G. & Emami, A. Localization of microscale devices in vivo using addressable transmitters operated as magnetic spins. *Nat. Biomed. Eng.* **1**, 736–744 (2017).

3.Sharma, S. *et al.* Location-aware ingestible microdevices for wireless monitoring of gastrointestinal dynamics. *Nat. Electron.* **6**, 242–256 (2023).

4.Qiu, M. *et al.* Novel concept of the smart NIR-light–controlled drug release of black phosphorus nanostructure for cancer therapy. *Proc. Natl. Acad. Sci.* **115**, 501–506 (2018).

5.Wang, X., Wang, C., Zhang, Q. & Cheng, Y. Near infrared light-responsive and injectable supramolecular hydrogels for on-demand drug delivery. *Chem. Commun.* **52**, 978–981 (2016).

6.Piraner, D. I. *et al.* Going Deeper: Biomolecular Tools for Acoustic and Magnetic Imaging and Control of Cellular Function. *Biochemistry* **56**, 5202–5209 (2017).

7.Tng, D. J. H., Hu, R., Song, P., Roy, I. & Yong, K.-T. Approaches and Challenges of Engineering Implantable Microelectromechanical Systems (MEMS) Drug Delivery Systems for in Vitro and in Vivo Applications. *Micromachines* **3**, 615–631 (2012).

8.Meng, E. & Sheybani, R. Insight: implantable medical devices. *Lab. Chip* **14**, 3233–3240 (2014).

9.Cobo, A., Sheybani, R. & Meng, E. MEMS: Enabled Drug Delivery Systems. *Adv. Healthc. Mater.* **4**, 969–982 (2015).

10.Maresca, D. *et al.* Biomolecular Ultrasound and Sonogenetics. *Annu. Rev. Chem. Biomol. Eng.* **9**, 229–252 (2018).

11.Walsby, A. E. Gas vesicles. *Microbiol. Mol. Biol. Rev.* **58**, 94–144 (1994).

12.Shapiro, M. G. *et al.* Biogenic gas nanostructures as ultrasonic molecular reporters. *Nat. Nanotechnol.* **9**, 311–316 (2014).

13.Sawyer, D. P. *et al.* Ultrasensitive ultrasound imaging of gene expression with signal unmixing. *Nat. Methods* **18**, 945–952 (2021).

14.Anthis, A. H. C. *et al.* Modular stimuli-responsive hydrogel sealants for early gastrointestinal leak detection and containment. *Nat. Commun.* **13**, 7311 (2022).

15.Lakshmanan, A. *et al.* Preparation of biogenic gas vesicle nanostructures for use as contrast agents for ultrasound and MRI. *Nat. Protoc.* **12**, 2050–2080 (2017).

16.Bourdeau, R. W. *et al.* Acoustic reporter genes for noninvasive imaging of microorganisms in mammalian hosts. *Nature* **553**, 86–90 (2018).

17.Wu, D. *et al.* Biomolecular actuators for genetically selective acoustic manipulation of cells. *Sci. Adv.* **9**, eadd9186 (2023).

18.Bar-Zion, A. *et al.* Acoustically triggered mechanotherapy using genetically encoded gas vesicles. *Nat. Nanotechnol.* **16**, 1403–1412 (2021).

19.Dutka, P. *et al.* Measuring gas vesicle dimensions by electron microscopy. *Protein Sci.* **30**, 1081–1086 (2021).

20.Hettiaratchi, M. H. *et al.* A rapid method for determining protein diffusion through hydrogels for regenerative medicine applications. *APL Bioeng.* **2**, (2018).

21.Dorshow, R. B. *et al.* Transdermal fluorescence detection of a dual fluorophore system for noninvasive point-of-care gastrointestinal permeability measurement. *Biomed. Opt. Express* **10**, 5103–5116 (2019).

22.Koester, S. T., Li, N., Lachance, D. M. & Dey, N. Marker-based assays for studying gut transit in gnotobiotic and conventional mouse models. *STAR Protoc.* **2**, 100938 (2021).

23.National Health Statistics Reports, Number 152, February 24, 2021. (2021).

24.Sands, B. E. & Kaplan, G. G. The role of TNFalpha in ulcerative colitis. *J. Clin. Pharmacol.* **47**, 930–941 (2007).

25.Wolfe, F., Caplan, L. & Michaud, K. Treatment for rheumatoid arthritis and the risk of hospitalization for pneumonia: associations with prednisone, disease-modifying antirheumatic drugs, and anti-tumor necrosis factor therapy. *Arthritis Rheum.* **54**, 628–634 (2006).

26.Sandborn, W. J. State-of-the-art: Immunosuppression and biologic therapy. *Dig. Dis. Basel Switz.* **28**, 536–542 (2010).

27.Kim, S. Y. & Solomon, D. H. Tumor necrosis factor blockade and the risk of viral infection. *Nat. Rev. Rheumatol.* **6**, 165–174 (2010).

28.Paiotti, A. P. R. *et al.* Effect of COX-2 inhibitor lumiracoxib and the TNF-α antagonist etanercept on TNBS-induced colitis in Wistar rats. *J. Mol. Histol.* **43**, 307–317 (2012).

29.Fries, W. *et al.* Infliximab and Etanercept Are Equally Effective in Reducing Enterocyte APOPTOSIS in Experimental Colitis. *Int. J. Med. Sci.* **5**, 169–180 (2008).

30.Popivanova, B. K. *et al.* Blocking TNF-α in mice reduces colorectal carcinogenesis associated with chronic colitis. *J. Clin. Invest.* **118**, 560–570 (2008).

31.Abasalizadeh, F. *et al.* Alginate-based hydrogels as drug delivery vehicles in cancer treatment and their applications in wound dressing and 3D bioprinting. *J. Biol. Eng.* **14**, 8 (2020).

32.Gaudio, E. *et al.* Dextran Sulfate Sodium (DSS) Colitis in Rats (Clinical, Structural, and Ultrastructural Aspects). *Dig. Dis. Sci.* **44**, 1458–1475 (1999).

33.Vargason, A. M., Anselmo, A. C. & Mitragotri, S. The evolution of commercial drug delivery technologies. *Nat. Biomed. Eng.* **5**, 951–967 (2021).

34.Amjadi, M., Kyung, K.-U., Park, I. & Sitti, M. Stretchable, Skin-Mountable, and Wearable Strain Sensors and Their Potential Applications: A Review. *Adv. Funct. Mater.* **26**, 1678–1698 (2016).

35.Lakshmanan, A. *et al.* Molecular Engineering of Acoustic Protein Nanostructures. *ACS Nano* **10**, 7314–7322 (2016).

36.Wang, C. *et al.* Bioadhesive ultrasound for long-term continuous imaging of diverse organs. *Science* **377**, 517–523 (2022).

37.Wang, C. *et al.* Monitoring of the central blood pressure waveform via a conformal ultrasonic device. *Nat. Biomed. Eng.* **2**, 687–695 (2018).

38.Wang, C. *et al.* Continuous monitoring of deep-tissue haemodynamics with stretchable ultrasonic phased arrays. *Nat. Biomed. Eng.* **5**, 749–758 (2021).

39.Hu, H. *et al.* Stretchable ultrasonic arrays for the three-dimensional mapping of the modulus of deep tissue. *Nat. Biomed. Eng.* 1–14 (2023) doi:10.1038/s41551-023-01038-w.

40.Rabut, C. *et al.* Ultrafast amplitude modulation for molecular and hemodynamic ultrasound imaging. *Appl. Phys. Lett.* **118**, 244102 (2021).

41.Maresca, D., Sawyer, D. P., Renaud, G., Lee-Gosselin, A. & Shapiro, M. G. Nonlinear X-Wave Ultrasound Imaging of Acoustic Biomolecules. *Phys. Rev. X* **8**, 041002 (2018).

42.Maresca, D. *et al.* Nonlinear ultrasound imaging of nanoscale acoustic biomolecules. *Appl. Phys. Lett.* **110**, 073704 (2017).

43.Holmes, D. L. & Stellwagen, N. C. Estimation of polyacrylamide gel pore size from Ferguson plots of normal and anomalously migrating DNA fragments. I. Gels containing 3 % N, N′-methylenebisacrylamide. *ELECTROPHORESIS* **12**, 253–263 (1991).

44.Klein, J., Stock, J. & Vorlop, K.-D. Pore size and properties of spherical Ca-alginate biocatalysts. *Eur. J. Appl. Microbiol. Biotechnol.* **18**, 86–91 (1983).

45.O'Toole, A., Lucci, M. & Korzenik, J. Inflammatory Bowel Disease Provoked by Etanercept: Report of 443 Possible Cases Combined from an IBD Referral Center and the FDA. *Dig. Dis. Sci.* **61**, 1772–1774 (2016).

46.Arnoult, C. *et al.* Crucial Role for Immune Complexes but Not FcRn in Immunization against Anti–TNF-α Antibodies after a Single Injection in Mice. *J. Immunol.* **199**, 418–424 (2017).

47.Irani, Y., Scotney, P., Nash, A. & Williams, K. A. Species Cross-Reactivity of Antibodies Used to Treat Ophthalmic Conditions. *Invest. Ophthalmol. Vis. Sci.* **57**, 586–591 (2016).

48.Dutka, P. *et al.* Structure of Anabaena flos-aquae gas vesicles revealed by cryo-ET. *Structure* **31**, 518-528.e6 (2023).

Chapter III

ULTRASOUND CONTROLLED SMART GV-HYDROGEL SYSTEMS

This chapter is both a summary of the future directions of my main project, with some preliminary unpublished results, and a review / reformat of relevant sections from two manuscripts that I co-authored highlighting other applications of GV-hydrogels that are not necessarily drug delivery related:

"Biomolecular actuators for genetically selective acoustic manipulation of cells" published by Wu D., Baresch D., Cook C., Ma Z., Duan M., Malounda D., Maresca D., Abundo M.P., Lee J., Shivaei S., Mittelstein D., Qiu T., Fischer P. and Shapiro M.G. in *Science Advances*

"Modular stimuli-responsive hydrogel sealants for early gastrointestinal leak detection and containment" published by Anthis A.H.C., Abundo M.P., Neuer A.L., Tsolaki E., Rosendorf J., Rduch T., Starsich F.H.L, Weisse B., Liska V., Schlegel A.A., Shapiro M.G. and Hermann I.K. in *Nature Communications*

3.1 Abstract

Hydrogels are prevalent in smart drug delivery systems owing to their biocompatibility, customizable properties, and high water content that allows for the efficient encapsulation of various therapeutics. However, they lack the ability to directly interact with ultrasound and cannot leverage on the strengths of the modality, namely its high penetration depth and spatiotemporal resolution. To overcome this, gas vesicles (GVs) have been integrated into hydrogel materials, enabling them to scatter ultrasound waves which provide contrast for imaging, and energy for material excitation or actuation. In this review, we explore some developments and applications of GV-hydrogel systems, showcasing their potential for deployment in a wide range of biomedical applications.

3.2 Introduction

Hydrogels have emerged as versatile materials in the development of drug delivery systems[1] and implants due to their highly hydrated polymer mesh that provides biocompatibility, and the ability to encapsulate and safely deploy a wide range of bioactive compounds ranging from small molecule drugs to peptides, antibodies, and cells. These platforms can often be engineered to be 'smarter' by enabling a response – typically in the hydrogel's micro and nanostructure – to environmental stimuli such as pH[2], temperature[3], and biomolecular concentration[4], or via exogenous energy sources such as, electrical[5], and magnetic fields[6–8], light[9,10] and ultrasound[11–13]. This high degree of customization in hydrogels has allowed them to consistently meet the diverse biomedical demands of cancer treatment, wound healing, and tissue engineering. However, whilst there have been significant efforts to engineer hydrogels with tunable material properties, the ability to image these hydrogel macromaterials and obtain consistent real-time readout of their location, structure and extracellular environment is often overlooked, making them less likely to be utilized in long-term treatments.

Ultrasound presents a promising solution in this regard, offering deep tissue penetration and high spatial precision at the micron scale[14], surpassing alternative optical and magnetic approaches. However, its use in smart bulk materials has mostly been limited to 'passive' approaches, relying instead on secondary heating effects[15] (hyperthermia) to activate hydrogels with a predetermined release profile, or by using cavitation which can be destructive. Furthermore, the similarity in densities between hydrogels and the extracellular matrix make it very challenging to monitor and image these soft devices *in vivo* with diagnostic ultrasound.

To address these challenges, ultrasound contrast agents in the form of gas vesicles [16–18](GVs) have been utilized in the development of various biomaterials. This enables generic hydrogels to readily interface with diagnostic ultrasound, enabling imaging and/or actuation. Through this review, we will explore the future directions and novel applications of GV-gels

and shed light on their advantages and potential for use in biomedical contexts like drug delivery, tissue culture and engineering, surgical seals and implants.

3.3 GVs-gels enable acoustically multiplexed payload release

Multiresponsive delivery systems offer a versatile approach by incorporating more than one release events or triggers. This capability can be harnessed to deploy multiple drugs that synergistically address complex conditions like heart disease[19]. By combining drugs with complementary mechanisms of action, multiresponsive systems have the potential to enhance therapeutic outcomes and overcome challenges associated with noncompliance. Additionally, these systems can enable multiple dosing of a single payload over time, which is particularly beneficial in extending the longevity of implants that deliver a full course of antibiotics or painkillers to facilitate wound healing. Such systems provide a flexible and efficient strategy for personalized medicine by allowing doctors to tailor the treatment type, dose, and drug release profiles to meet specific patient needs.

Multiplexed payload release from GV-gels can be accomplished by utilizing different species of gas vesicles. GVs harvested from different host species possess different critical collapse pressures[20] (**Fig. 1, a-c**). By strategically collapsing the GVs in a specific order, it becomes possible to trigger the formation of increasingly larger pores within the gel matrix to influence the individual solute diffusivities. To test this, BSA diffusion through a hydrogel containing two GVs, namely Ana (WT) and Ana (ΔGvpC), was evaluated. The Ana GVs chosen were of roughly similar sizes but possess different acoustic collapse pressures, ~600 kPa for ΔGvpC and ~700 kPa for WT. We see from preliminary data that BSA diffusion increases in a stepwise manner in response to a specific GV-population getting collapsed (**Fig. 2**).

With this platform, it becomes possible to simultaneously carry out slow, long-term release of small nonsteroidal anti-inflammatory molecule and fast, short-term release of macromolecular therapeutic antibodies within the same system. Furthermore, since this approach has already been previously employed for multiplexed ultrasound imaging and

signal collection (**Fig. 1d**), these GV-gels will make it possible for doctors to visualize the release progress as a function of the remaining ultrasound signal within the hydrogel.

In the future, drugs can also be tethered to the GV-itself using mechanophores[21] that will dissociate (from the GV) once activated, thereby enabling non-porosity based multiplexed payload release and multi-dose treatments. This is an ongoing research area in our lab with some promising unpublished results.

Overall, this sequential collapse mechanism offers precise control over the release of encapsulated substances, allowing for a multiplexed release strategy that can be monitored and tailored to the desired application and release kinetics. The wide range of collapse pressures accessible via the large GV opens new possibilities for the design and optimization of drug delivery systems using ultrasound.

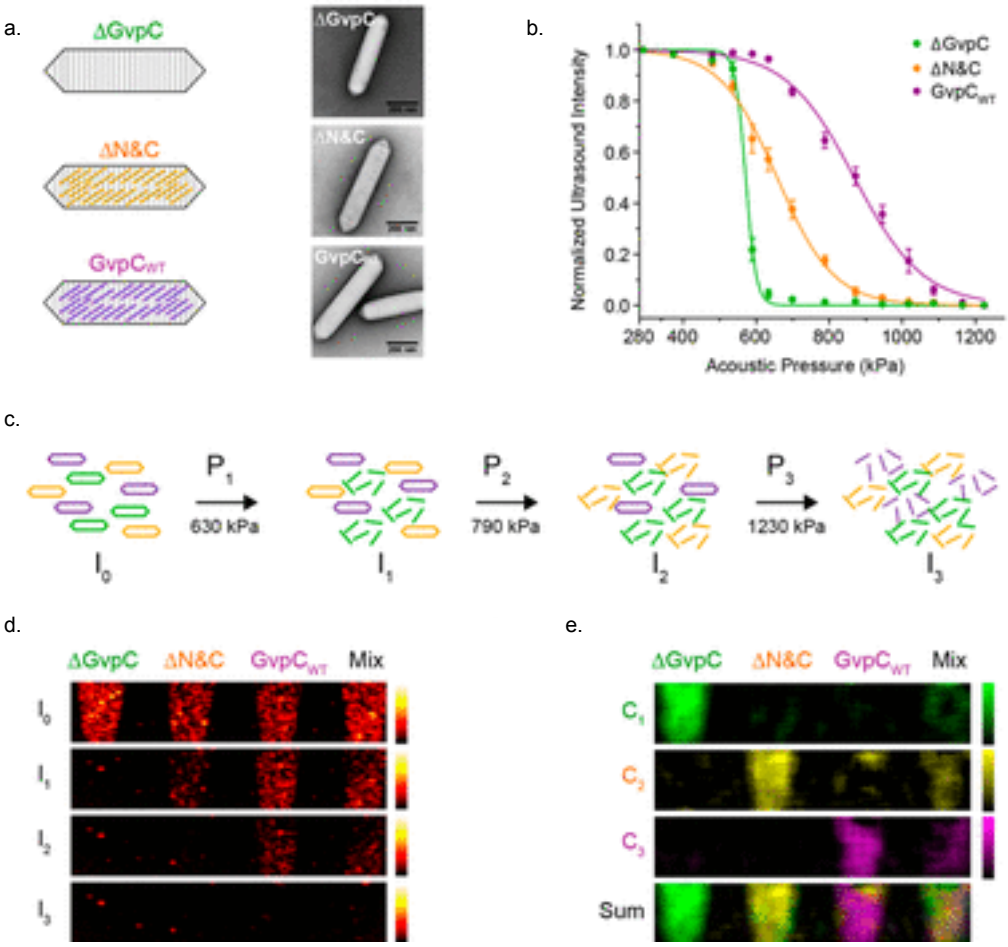

Figure 1 – Adapted and Reproduced from Lakshmanan A. et al (2016)[20], Acoustic multiplexing using different GV variants

a, Schematic illustration of the three engineered GV variants used for acoustic multiplexing. ΔGvpC, ΔN&C, and GvpCWT variants are represented by green, orange, and purple colors, respectively. Accompanying TEM images show the conservation of GV shape among the three variants (scale bars are 200 nm). **b,** Acoustic collapse curves for the GV variants showing normalized ultrasound signal intensity as a function of increasing peak positive pressure from 290 kPa to 1.23 MPa (N = 3 independent trials, error bars are SEM). **c,** Schematic illustration of acoustic spectral unmixing, showing serial collapse of

the GV variants based on their critical collapse pressure and indicating the pressures used in panels f and g. **d,** Ultrasound images of an agarose phantom containing wells with ΔGvpC, ΔN&C, GvpCWT and a mixture of the three variants (all GVs at final OD 1.0 in PBS), acquired at 6.25 MHz. I0, before collapse; I1, after collapse at 630 kPa I2: after collapse at 790 kPa I3: after collapse at 1230 kPa. **e,** Spectrally unmixed images processed from the raw ultrasound data in (d).

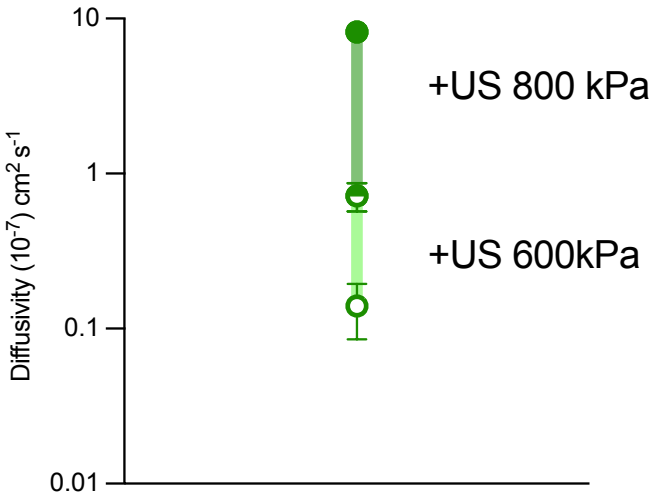

Figure 2 – GVs-gels enable acoustically multiplexed BSA diffusivity

5% Clustered Ana ΔGvpC (acoustic collapse pressure ~600 kPa) and 10% Clustered Ana WT (acoustic collapse pressure ~700 kPa) was embedded in 10% polyacrylamide hydrogel. The diffusivity coefficient of BSA-AlexaFluor 647 during the stepwise application of ultrasound, first at 600 kPa, then at 800 kPa, is shown here.

3.4 GV-gels can be tuned to deliver payloads across length scales

The field of drug delivery encompasses a diverse range of therapeutics[22], spanning a wide length scale from approximately 0.5 nm in small molecules, proteins, peptides, antibodies, and nucleic acids, to 1 μm in the case of cells (**Fig. 3**). Not only do these therapeutics vary in size, but their stabilities, selectivities, and reactivity also differ significantly. Despite the unique delivery challenges associated with the different types of therapeutics, hydrogels continue to play a prominent role in drug delivery platforms due to their biocompatibility and tunable mesh sizes ranging from 10 nm to 1 μm.

Similarly, the shapes and sizes of gas vesicles can be altered depending on the host organism and the growth conditions, allowing us to harvest purified gas vesicles with lengths of ~ 10 nm (bicones[23], **Fig. 4**) up to a ~ 1 μm when expressed in mammalian cells (spindles[24], **Fig. 5**). The wide range of accessible GV sizes and its hydrophilic exterior lends itself well to being incorporated in a variety of existing hydrogel drug delivery systems and can be tuned specifically to accommodate various therapeutic payloads.

We tested the ability of GV-gels to modulate the diffusivity of three cargos of different sizes: AlexaFluor 647 (r ~ 0.5 nm), BSA (r ~ 5 nm), IgG (r ~ 10 nm) and 50 nm quantum dots, in three hydrogels of different mesh sizes: alginate (r ~ 5 nm), polyacrylamide (r ~ 20 nm) and agarose (r~ 100 nm) respectively. In these preliminary experiments, diffusivity switching behavior was observed, highlighting its potential for use with other therapeutic classes (**Fig. 6**).

More experiments will have to be carried out to optimize the dynamic range of the behavior depending on the chosen drug cargo, and ultrasound imaging parameters will have to be specifically tuned if newer, less documented GV-types are going to be considered for deployment in synthetic materials. Nevertheless, the versatility of GVs will allow them to be easily incorporated in the many clinically approved hydrogel drug delivery systems.

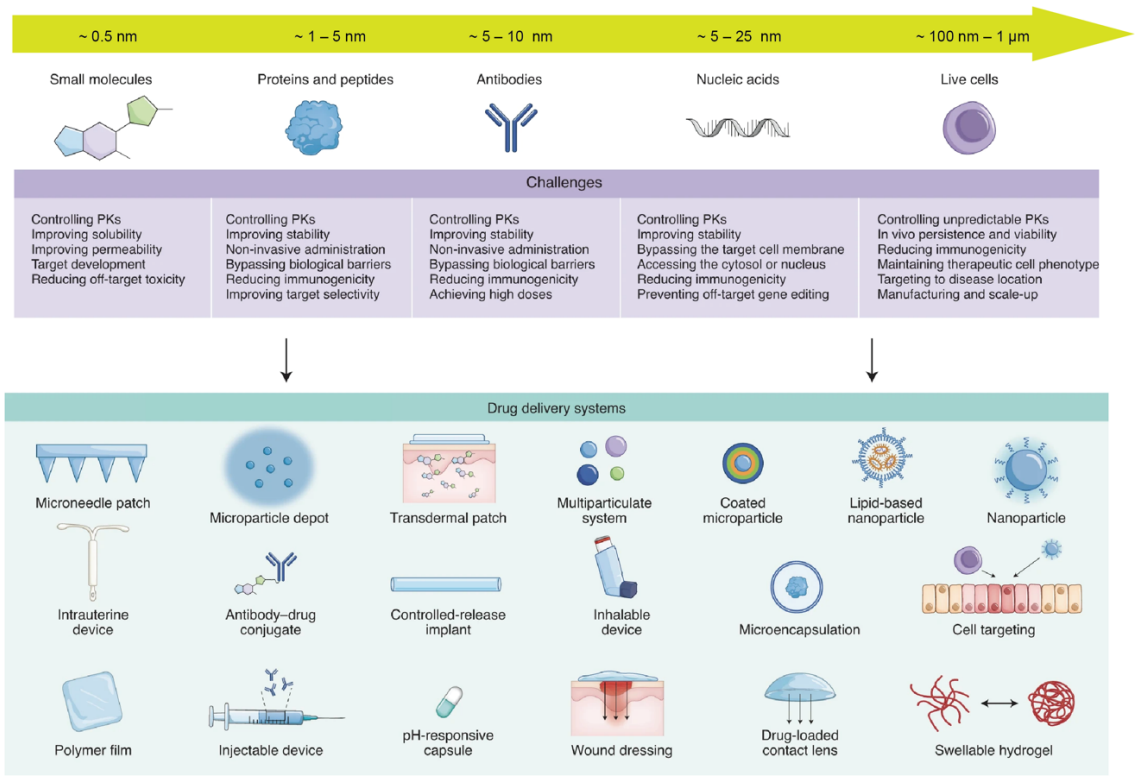

Figure 3[22] – Adapted from Vargason A.M., et al (2021), Classes of therapeutic and delivery paradigms

Each of the five generations of therapeutic (small molecules, proteins and peptides, antibodies, nucleic acids and cell therapies (live cells)) have their unique delivery challenges. Regardless of the class of therapeutic, drug delivery systems have adopted one or more strategies for drug modification or environmental modification.

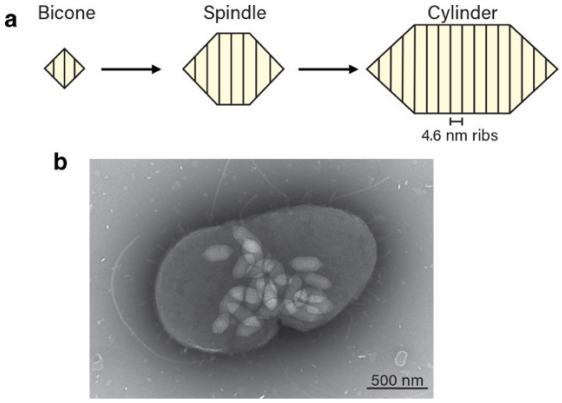

Figure 4 – Reproduced from Hill A.M. and Salmond G.P.C. [23](2020), Gas vesicle development and appearance.

a, Gas vesicles develop from small bicone structures into mature spindle/cylindrical structures. **b,** Transmission electron micrograph of mature gas vesicles inside a *Serratia* sp. ATCC 39006 cell.

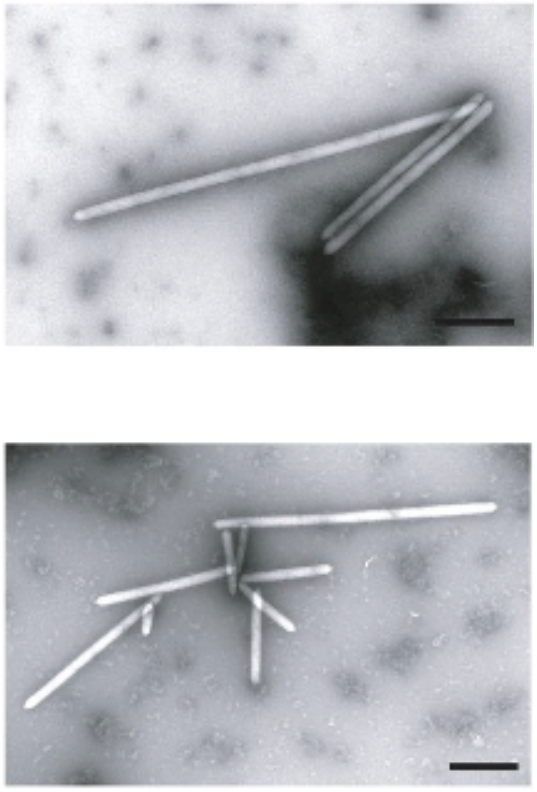

Figure 5 – Reproduced and adapted from Farhadi A. et al (2019)[24], Ultrasound imaging of gene expression in mammalian cells

(Top) Representative TEM image of purified gas vesicles expressed in HEK293T cells. (Bottom) Representative TEM image of gas vesicles purified from HEK293T cells transiently transfected with mARGs for 72 hours. All scale bars represent 500 nm.

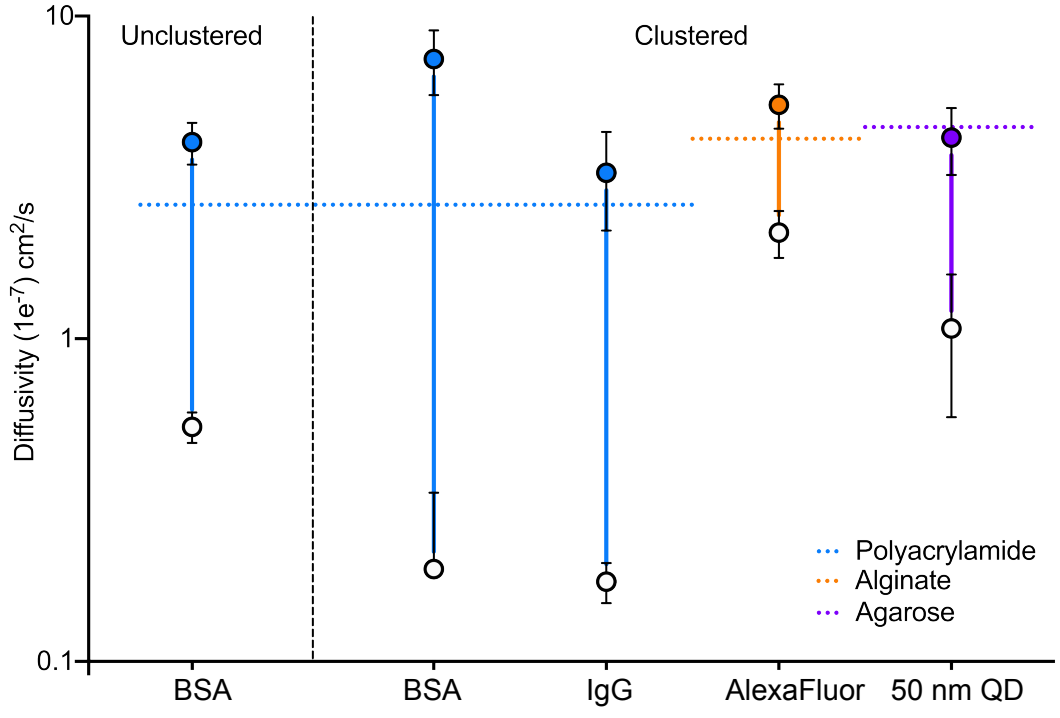

Figure 6 – GV-gels produce ultrasound modulated diffusivity effects in a wide size range of solute and polymer candidates

Diffusivity of the solutes was tracked through fluorescence evolution in a thin capillary. AlexaFluor 647 was conjugated to BSA. IgG conjugated to AlexaFluor 488 was purchased from Sigma-Aldrich (16-240) and used as is. Alexa 647 was use as is. The quantum dots (QD) was purchased and used as is.

3.5 GVs enable biomaterial patterning using acoustic radiation force

The microstructure of hydrogels plays a significant role in determining the mechanical and transport properties of biomaterials used in drug delivery implants and tissue scaffolds. Bulk material characteristics such as porosity, stress and strain modulus are influenced by the arrangement of polymer molecules, which is established during the synthesis process. This underscores the importance of carefully selecting the initial polymer system when designing biomaterials, as replacing these soft devices can be an invasive procedure requiring surgical intervention. Additionally, the distribution and arrangement of therapeutics within the hydrogel matrix can also affect performance[25]. Strategic placement of drug-containing depots within the implants is crucial to ensuring optimal pharmacokinetics upon drug release. However, since hydrogels degrade[26] when exposed to the proteolytic environment *in vivo*, the predetermined material properties lose their relevance over time, which could negatively affect therapeutic outcomes if not correctly accounted for. Therefore, having the ability to remotely manipulate and control the microarchitecture in materials[7] noninvasively after deployment will enable the development of more precise, dynamic and adaptive treatments.

Acoustic radiation force (ARF)[27] enables the manipulation of objects that possess different densities or compressibilities compared to their surrounding medium using ultrasound. This has been successfully exploited to manipulate and arrange micron-sized synthetic particles and large mammalian cells. However, this is level of control is difficult to replicate in nanometer sized objects like polymers, peptides, and antibodies due to their small size, i.e., $F_{ARF} \sim O(r^3)$, and weak acoustic contrast relative to water. This makes achieving precise microstructure control and patterning of therapeutics within hydrogels a challenge unless supplemented by ARF actuators like GVs.

Since GVs are 97% air due to their gas core[28], they possess markedly different densities and compressibilities relative to aqueous media that allow them to experience ARF despite being nanometer sized. ARF on GVs was also found to act in the opposite direction from other biomaterials by virtue of being less dense than water (**Fig. 7f**). This difference is critical in allowing the selective manipulation of objects that are labelled with GVs.

To test the ability of GVs to be patterned in 3D space, we created an acoustic hologram using a single-element 3.5-MHz transducer and a 3D-printed phase mask designed to produce an "R"-shaped pressure profile (**Fig. 8h**). We applied this hologram to acoustic bacteria suspended in an agarose solution that can be solidified at cold temperatures to form a gel. As expected, the bacteria were immobilized inside the gel in the desired spatial pattern (**Fig. 8i**). As an added feature, the spatial distribution of GV-expressing cells could be imaged with ultrasound (**Fig. 8j**), providing a means to verify patterning in optically opaque media. These results demonstrate the ability of GVs to enable the acoustic trapping, patterning, and dynamic rearrangement of engineered bacteria, and the rapid biofabrication of living materials.

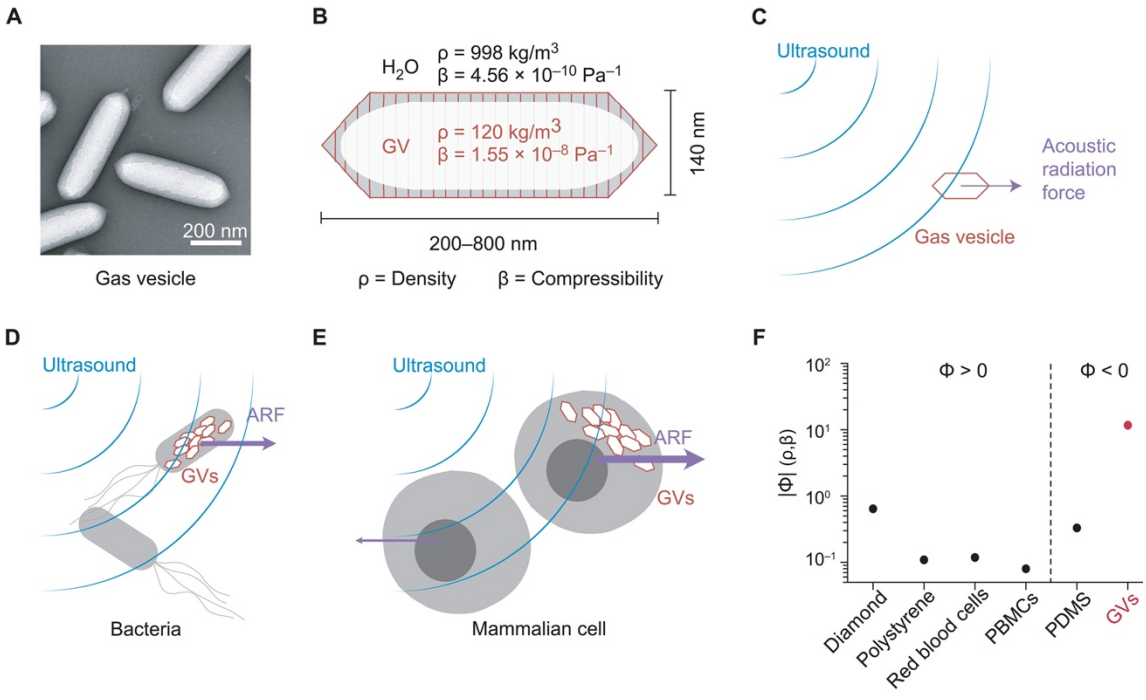

Figure 7 – Reproduced from Wu D., et al (2023)[29], GVs as biomolecular transducers of ARF.

a, Transmission electron microscopy (TEM) image of representative GVs from A. flos-aquae. **b,** Schematic drawing of a GV, showing its effective density (ρ) and compressibility (β) relative to that of the surrounding water. **c,** Illustration of a GV experiencing ARF due to applied ultrasound. **d,** Illustration of a bacterium experiencing enhanced ARF due to intracellular GVs. **e,** Illustration of a mammalian cell experiencing a unique ARF compared to a wild-type cell due to intracellular GVs. **f,** Estimated magnitude of the acoustic contrast factor, |Φ|, of GVs and several common materials used in acoustic manipulation. Materials to the left and right of the vertical dashed line exhibit positive and negative acoustic contrast in water, respectively. PBMCs, peripheral blood mononuclear cells; PDMS, polydimethylsiloxane.

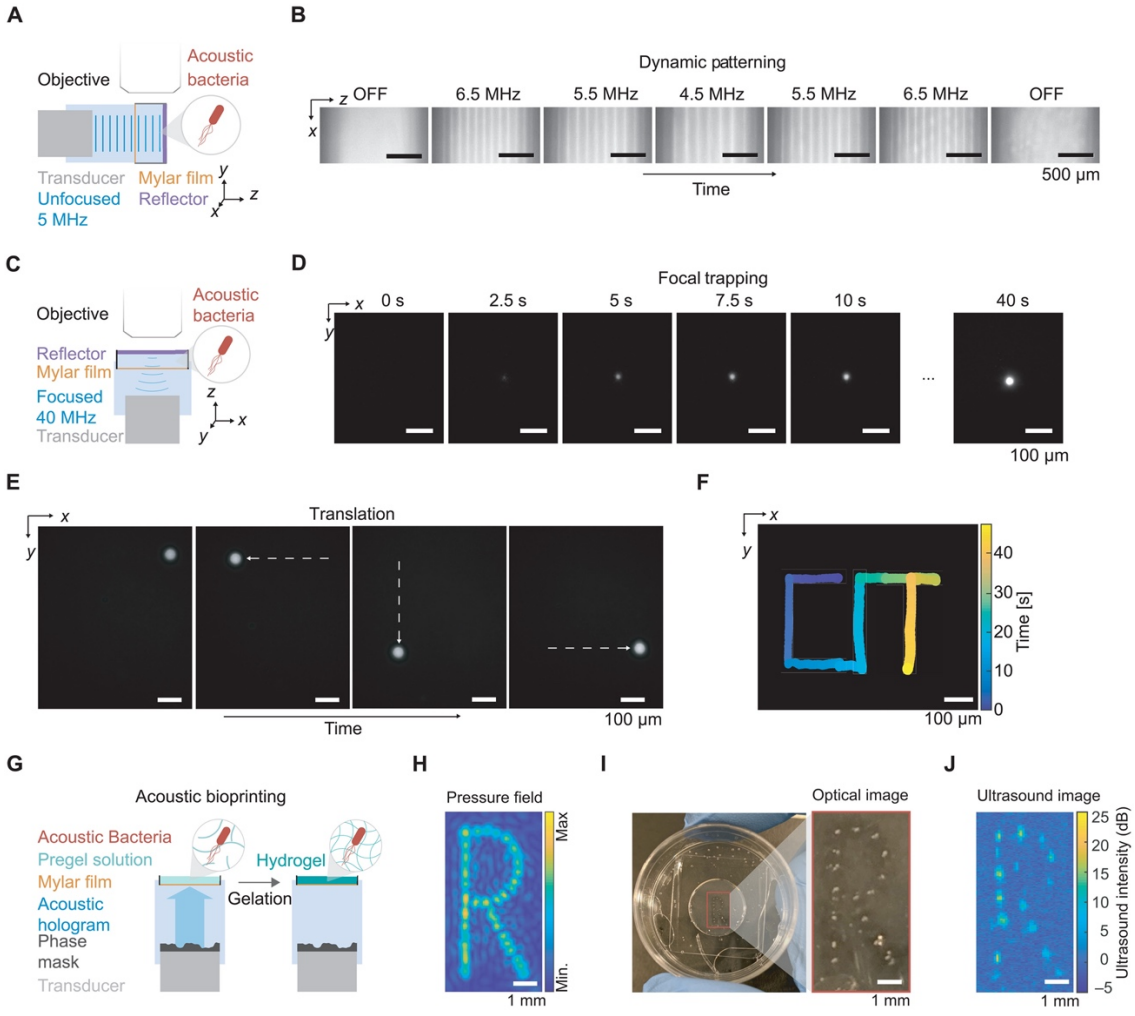

Figure 8 – Reproduced from Wu D., et al (2023)[29], Dynamic patterning and one-step bioprinting with acoustic bacteria.

a, Diagram of the acoustic chamber setup for frequency-controlled spatial patterning. A transducer is aligned orthogonal to a glass reflector using a 3D-printed holder. The sound wave passes through a Mylar membrane, is reflected by the glass reflector, and forms a standing wave near the reflector. The sample region containing acoustic E. coli is imaged using an epifluorescence microscope. **b,** Sequential fluorescence images of acoustic E. coli in the presence of an acoustic standing wave at varying frequencies. Frequencies were changed every 50 s. **c,** Diagram of the acoustic chamber setup for image-guided trapping and positioning of acoustic E. coli. Imaging is performed along the axis of a focused 40-

MHz transducer. **d,** Sequential fluorescence images of the formation of a cluster of acoustic E. coli at the ultrasound focus. **e,** Fluorescence images of a cluster of acoustic E. coli positioned at distinct locations in the x-y plane. The positioning is controlled by the translation of the transducer in the x-y plane using a micromanipulator and is guided by real-time fluorescence imaging of the bacteria. **f,** Overlaid positions of the cell cluster, color-coded by time, to form a spatiotemporal pattern writing out "CIT." **g,** Diagram of the process for acoustic biofabrication. A transducer and phase mask is aligned such that the acoustic hologram is formed inside the sample chamber containing acoustic E. coli suspended in low-melt agarose solution. The gelation of the agarose is triggered to immobilize the acoustically patterned E. coli. **h,** Simulated pressure amplitude generated by the acoustic hologram. **i,** Acoustically patterned E. coli embedded in agarose gel. **j,** Ultrasound image of acoustically patterned E. coli.

3.6 GVs embedded in sealants enable post-surgical leak detection with ultrasound

Hydrogels play a crucial role in supporting the healing process of sutures after surgery by providing mechanical support through their high tensile strength, sealing capabilities with their adhesive and bioactive properties[30], and facilitating the controlled release of therapeutics for wound healing. However, in the event of a breach in the suture line, these hydrogel implants are unable to serve as preventive measures to completely halt or eliminate full-blown leaks, which can lead to severe health complications and high mortality rates[31]. Therefore, it becomes highly desirable to enhance these hydrogel implants with on-demand sensing and readout capabilities. By incorporating sensors or indicators within the hydrogel matrix, these implants could detect leaks early on and provide real-time alerts to healthcare professionals.

We designed one such hydrogel implant utilizing GVs embedded in a polyacrylamide gel as one of the two sensors to indicate leak originating from a hole in the abdomen (**Fig. 9, b-d**). Upon exposure to intestinal fluid (from the leak), the hydrogel implant 'TurnOFF' loses its ultrasound contrast as the proteases cleave the embedded GVs leading to GV collapse, and consequently a loss in ultrasound signal (**Fig. 10d**) within 2 hours. This early detection would enable prompt intervention and treatment, potentially preventing further complications and improving patient outcomes.

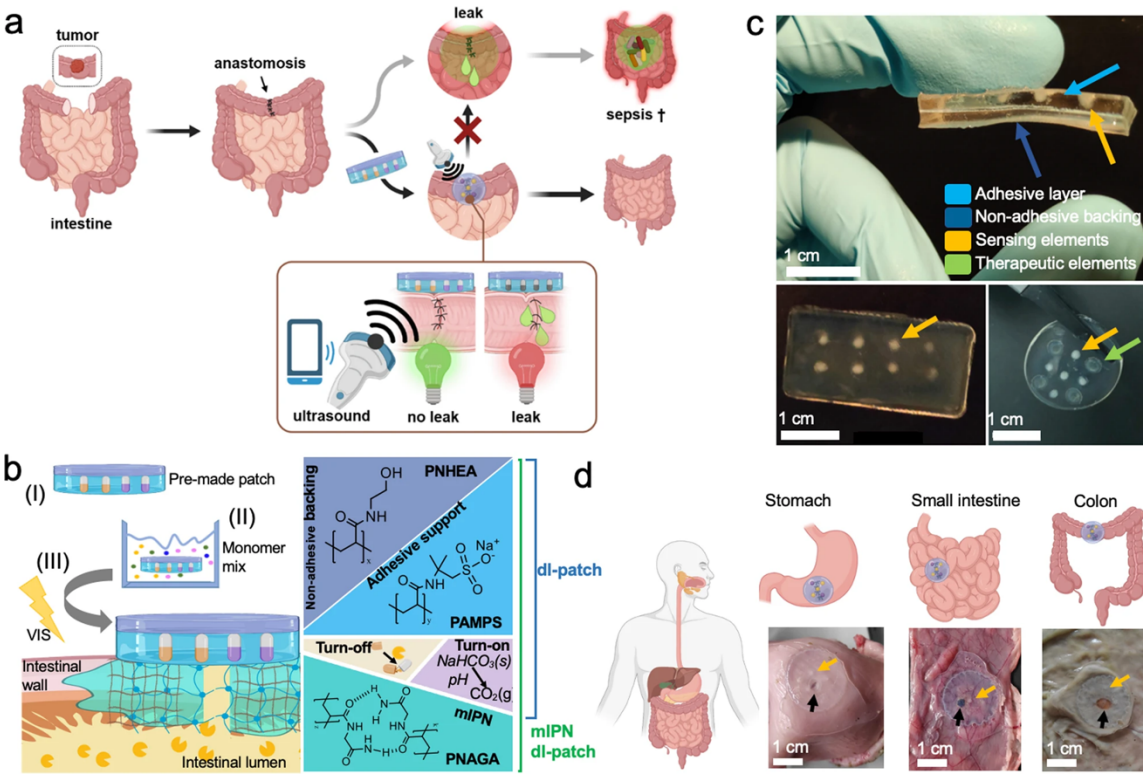

Figure 9 – Reproduced from Anthis A. H. C. et al (2022)[32]

a, Envisaged application of the leak-detecting sealant hydrogel patches enabling non-invasive postoperative surveillance of anastomoses using port-able, pocket handheld ultrasound probes (cross denotes high mortality of developed sepsis). **b**, Composition of the layered-leak detecting sealant hydrogel patch, composed of a non-adhesive backing (PNHEA), adhesive suture support layer (PAMPS), sensing elements (TurnOFF sens-ing elements comprising enzyme-digestible gas vesicles or TurnON elements comprising pH-reactive sodium bicarbonate) attached to tissue via the formation of a mutually interpenetrating network (mIPN). b-I Application of the as-prepared hydrogel patch, which is incubated in a 33 wt% NAGA monomer/water solution containing LAP initiator (b-II) and finally is attached to tissue using visible light to form an mIPN (lightning denotes light) (b-III). **c**, As-prepared hy-drogels, manufactured in various shapes, exhibit discrete layers and compartments, namely adhesive support (light blue arrow), non-adhesive backing (dark blue arrow), TurnOFF Halo gas vesicles sensing elements (5 µL 20 vol%,

orange arrow) and 2.5 mg/mL ZnO in PAAm an-tibacterial elements (green arrow). **d**, Illustration showcasing gastrointestinal organs and the application of the hydrogel patches containing sensing elements (orange arrow) on the outer lining of porcine stomach, small intestine and colon, each closing a 4 mm defect (black arrow). Figure wide color coding: light blue—adhesive support, dark blue—non-adhesive backing, yellow—Turn-OFF sensing element, purple—TurnON sensing element, turquoise green—mIPN. Figures 5 **a, b, d** has been created using biorender.com.

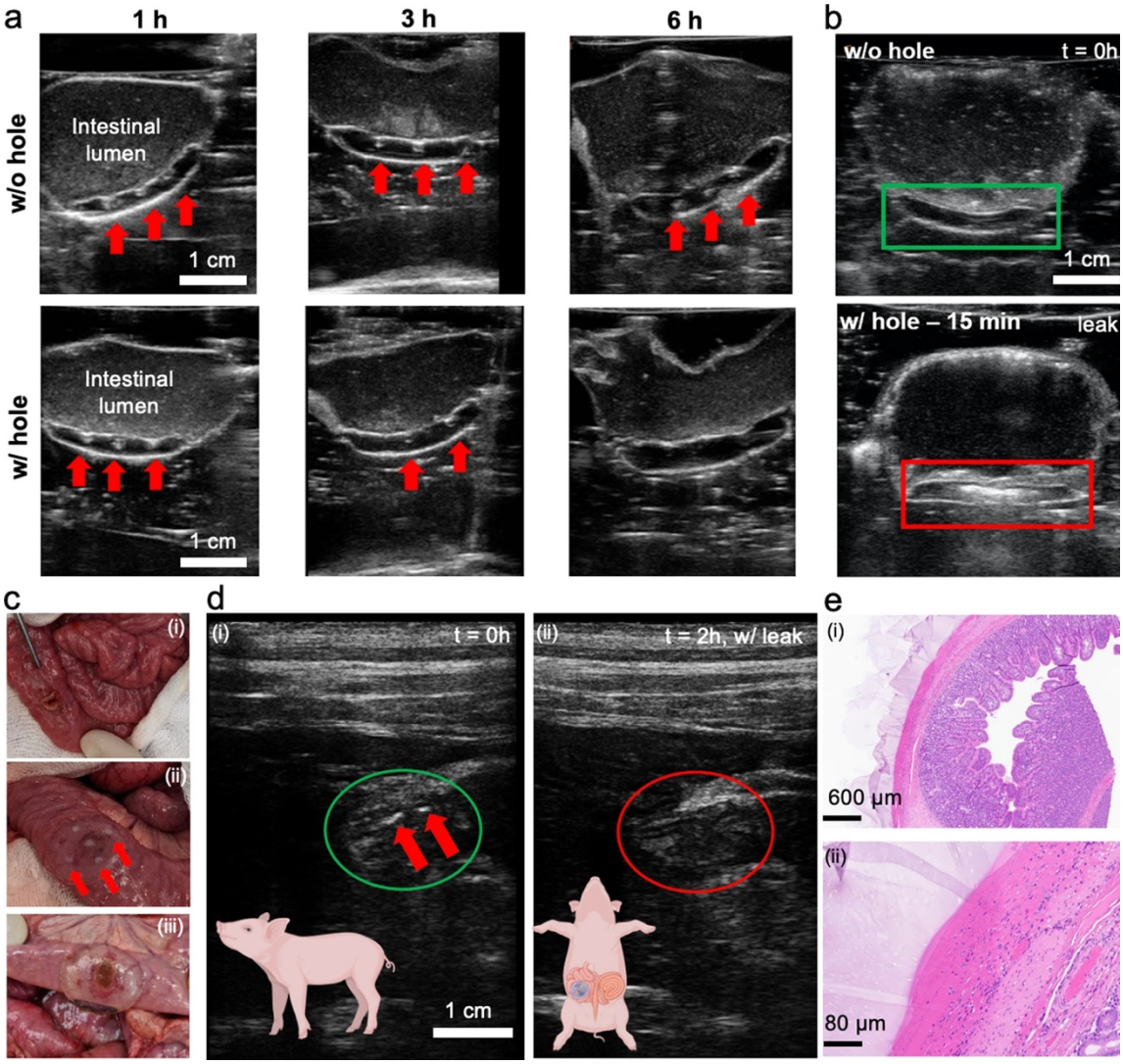

Figure 10 – Reproduced from Anthis A. H. C. et al (2022)[32]

a, Ex vivo ultrasound images obtained using an ipad controlled Clarius L7 HD probe of (a) TurnOFF patterned hydrogel patch attached to intestine filled with SIF, equipped with a 4 mm hole simulating the perforation. The suture sites are monitored over six hours, showcasing pattern disappearance, $N \geq 3$. **b**, TurnON sensing element equipped hydrogel patch attached to an intestinal tissue model, filled with SGF indicating suture perforation by increased ultrasound scattering after fifteen minutes of contact with SGF, $n \geq 3$. **c,** In vivo application of TurnOFF DL-patches on piglet intestine with a defect. c-i 4 mm defect formation on live small porcine intestine. c-ii photograph of patch immediately after

application on the defect. Sensing elements are clearly visible (red arrows). c-iii sealant patch 2 h post application on formed defect, presenting containment of digestive leak. **d**, Ultrasound data recorded (d-i) immediately after patch application and surgical closure of the abdomen with a running suture. Sensing elements are discernible (red arrows). (ii), (d-ii) 2 h after application, sensing elements were not detectable anymore, in line with the disappearance of the opaque dots (c-iii). **e**, Histological micrographs of intestinal tissue collected after euthanasia of the piglet shows firm attachment of the hydrogel to the serosa of the small intestine tissue and no visible tissue damage. Two samples were analysed yielding visually indistinguishable results. Figure wide color coding: red arrows—TurnOFF sensing element active. Figure **d** has been created using biorender.com.

3.7 References

1.Vigata, M., Meinert, C., Hutmacher, D. W. & Bock, N. Hydrogels as Drug Delivery Systems: A Review of Current Characterization and Evaluation Techniques. *Pharmaceutics* **12**, 1188 (2020).

2.Gupta, P., Vermani, K. & Garg, S. Hydrogels: from controlled release to pH-responsive drug delivery. *Drug Discov. Today* **7**, 569–579 (2002).

3.Ramanan, R. M. K., Chellamuthu, P., Tang, L. & Nguyen, K. T. Development of a Temperature-Sensitive Composite Hydrogel for Drug Delivery Applications. *Biotechnol. Prog.* **22**, 118–125 (2006).

4.Shahriari, M. *et al.* Enzyme responsive drug delivery systems in cancer treatment. *J. Controlled Release* **308**, 172–189 (2019).

5.Svirskis, D., Travas-Sejdic, J., Rodgers, A. & Garg, S. Electrochemically controlled drug delivery based on intrinsically conducting polymers. *J. Controlled Release* **146**, 6–15 (2010).

6.Kost, J., Wolfrum, J. & Langer, R. Magnetically enhanced insulin release in diabetic rats. *J. Biomed. Mater. Res.* **21**, 1367–1373 (1987).

7.Zhao, X. *et al.* Active scaffolds for on-demand drug and cell delivery. *Proc. Natl. Acad. Sci.* **108**, 67–72 (2011).

8.Qin, J. *et al.* Injectable Superparamagnetic Ferrogels for Controlled Release of Hydrophobic Drugs. *Adv. Mater.* **21**, 1354–1357 (2009).

9.Zhan, C. *et al.* Phototriggered Local Anesthesia. *Nano Lett.* **16**, 177–181 (2016).

10.Timko, B. P. *et al.* Near-infrared–actuated devices for remotely controlled drug delivery. *Proc. Natl. Acad. Sci.* **111**, 1349–1354 (2014).

11.Sun, Z., Song, C., Wang, C., Hu, Y. & Wu, J. Hydrogel-Based Controlled Drug Delivery for Cancer Treatment: A Review. *Mol. Pharm.* **17**, 373–391 (2020).

12.Kubota, T., Kurashina, Y., Zhao, J., Ando, K. & Onoe, H. Ultrasound-triggered on-demand drug delivery using hydrogel microbeads with release enhancer. *Mater. Des.* **203**, 109580 (2021).

13.Epstein-Barash, H. *et al.* A microcomposite hydrogel for repeated on-demand ultrasound-triggered drug delivery. *Biomaterials* **31**, 5208–5217 (2010).

14.Maresca, D. *et al.* Biomolecular Ultrasound and Sonogenetics. *Annu. Rev. Chem. Biomol. Eng.* **9**, 229–252 (2018).

15.Sirsi, S. R. & Borden, M. A. State-of-the-art materials for ultrasound-triggered drug delivery. *Adv. Drug Deliv. Rev.* **72**, 3–14 (2014).

16.Walsby, A. E. Gas vesicles. *Microbiol. Mol. Biol. Rev.* **58**, 94–144 (1994).

17.Shapiro, M. G. *et al.* Biogenic gas nanostructures as ultrasonic molecular reporters. *Nat. Nanotechnol.* **9**, 311–316 (2014).

18.Bourdeau, R. W. *et al.* Acoustic reporter genes for noninvasive imaging of microorganisms in mammalian hosts. *Nature* **553**, 86–90 (2018).

19.Piña, I. L. Risks and benefits of a multidrug approach to mild-to-moderate heart failure. *Am. J. Med.* **110**, 63–67 (2001).

20.Lakshmanan, A. *et al.* Molecular Engineering of Acoustic Protein Nanostructures. *ACS Nano* **10**, 7314–7322 (2016).

21.P. Kabb, C., S. O'Bryan, C., D. Morley, C., E. Angelini, T. & S. Sumerlin, B. Anthracene-based mechanophores for compression-activated fluorescence in polymeric networks. *Chem. Sci.* **10**, 7702–7708 (2019).

22.Vargason, A. M., Anselmo, A. C. & Mitragotri, S. The evolution of commercial drug delivery technologies. *Nat. Biomed. Eng.* **5**, 951–967 (2021).

23.Hill, A. M. & Salmond, G. P. C. Microbial gas vesicles as nanotechnology tools: exploiting intracellular organelles for translational utility in biotechnology, medicine and the environment. *Microbiology* **166**, 501–509 (2020).

24.Farhadi, A., Ho, G. H., Sawyer, D. P., Bourdeau, R. W. & Shapiro, M. G. Ultrasound imaging of gene expression in mammalian cells. *Science* **365**, 1469–1475 (2019).

25.Annabi, N. *et al.* Controlling the Porosity and Microarchitecture of Hydrogels for Tissue Engineering. *Tissue Eng. Part B Rev.* **16**, 371–383 (2010).

26.El-Sherbiny, I. M. & Yacoub, M. H. Hydrogel scaffolds for tissue engineering: Progress and challenges. *Glob. Cardiol. Sci. Pract.* **2013**, 316–342 (2013).

27.Torr, G. R. The acoustic radiation force. *Am. J. Phys.* **52**, 402–408 (1984).

28.Lakshmanan, A. *et al.* Preparation of biogenic gas vesicle nanostructures for use as contrast agents for ultrasound and MRI. *Nat. Protoc.* **12**, 2050–2080 (2017).

29.Wu, D. *et al.* Biomolecular actuators for genetically selective acoustic manipulation of cells. *Sci. Adv.* **9**, eadd9186 (2023).

30.Gao, L. *et al.* A novel dual-adhesive and bioactive hydrogel activated by bioglass for wound healing. *NPG Asia Mater.* **11**, 1–11 (2019).

31.Choudhuri, A. H. & Uppal, R. Predictors of septic shock following anastomotic leak after major gastrointestinal surgery: An audit from a tertiary care institute. *Indian J. Crit. Care Med. Peer-Rev. Off. Publ. Indian Soc. Crit. Care Med.* **17**, 298–303 (2013).

32.Anthis, A. H. C. *et al.* Modular stimuli-responsive hydrogel sealants for early gastrointestinal leak detection and containment. *Nat. Commun.* **13**, 7311 (2022).